Electronic Supplementary Material (ESI) for ChemComm.

Extremely Twisted and Bent Pyrene-Fused N-Heterocyclic Germylenes

Kelsie E. Krantz, [a] Sarah L. Weisflog, [a] Wenlong Yang, [a] Diane A. Dickie, [a] Nathan C. Frey, [b] Charles Edwin Webster, [b]* Robert J. Gilliard, Jr[a]*

[a]Department of Chemistry, University of Virginia, 409 McCormick Rd., PO Box 400319, Charlottesville, VA 22904

[b]Department of Chemistry, Mississippi State University, Box 9573, Mississippi State, MS 39762

[*]To whom correspondence should be addressed: rjg8s@virginia.edu, ewebster@chemistry.msstate.edu.

Supporting Information

Table of Contents

General Procedures

All manipulations involving air- and moisture-sensitive compounds were carried out under inert atmosphere of purified argon using an MBRAUN LABmaster glovebox equipped with a -37 °C freezer, or standard Schlenk line techniques. All solvents were purified by distillation over sodium and benzophenone. Glassware was oven-dried at 190 °C overnight. The NMR spectra were recorded at room temperature on a Bruker Advance 600 MHz spectrometer. Proton and carbon chemical shifts are reported in ppm and are referenced using the residual proton and carbon signals of the deuterated solvent (^{1}H; C_6D_6, δ 7.16; ^{13}C; δ 128.1 ppm). Single crystal X-ray diffraction data was collected on a Bruker Kappa APEXII diffractometer. The structures were solved and refined using the Bruker SHELXTL Software Package within APEX3 and OLEX2. The UV-visible spectra were recorded on a Cary 60 UV-vis Spectrophotometer with a resolution of 0.5 nm. Sample solutions were prepared in toluene in a 1 cm square air-free quartz cuvette. The IR spectra were recorded in the solid-state on a Cary 630 FTIR Spectrometer with attached Diamond ATR accessory. Deuterated solvents were purchased from Cambridge Isotope Laboratories. Suitable elemental analysis could not be obtained due to the reactivity of the products. The 1,3-bis(2,6-diiso-propylphenyl)imidazolium chloride (IPr•HCl),[1] 4,5,9,10-tetrabromo-2,7-di-tert-butylpyrene,[2] and 1,3-diisopropyl-4,5-dimethylimidazol-2-ylidene (sIPr)[3] were prepared according to the literature procedure.

Experimental Procedures

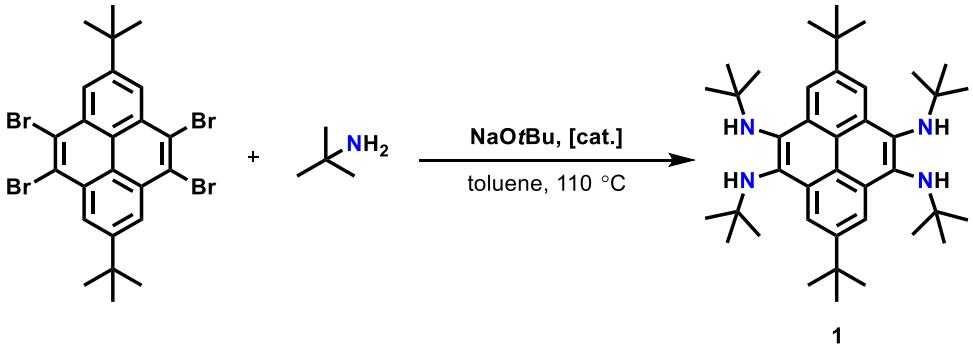

1

Synthesis of Compound 1. In a 50 mL flask, 1,3-bis(2,6-diiso-propylphenyl)imidazolium chloride (IPr•HCl, 0.471 g, 1.11 mmol), [Pd(OAc)$_2$] (0.124 g, 0.554 mmol), and NaO*t*Bu (0.160 g, 1.66 mmol) were stirred in 20 mL of toluene at room temperature for 1 hr until a clear orange solution was observed. In a Schlenk tube 4,5,9,10-tetrabromo-2,7-di-tert-butylpyrene (5.00 g, 7.91 mmol) and NaO*t*Bu (3.65 g, 38.0 mmol) were dissolved in anhydrous toluene (100 mL). The previous solution was added to the Schlenk tube, and tert-butylamine (3.99 mL, 38.0 mmol) was added under positive argon pressure. The resulting dark orange solution was stirred at 110 °C for 16 hrs. The mixture was cooled to room temperature and filtered over celite. The solvent was removed from the filtrate to leave a dark orange solid. The crude solid was washed with hexanes (3 x 20 mL) to yield the pure yellow product (4.41 g, 93% yield). Colorless block-shaped crystals suitable for X-ray diffraction studies were obtained from a concentrated hexane solution at -37 °C. ^{1}H NMR (600 MHz, C_6D_6, 298 K) δ = 8.85 (s, 4H, CH_{pyr}), 4.23 (br. s, 4H, NH), 1.65 (s, 18H, C(CH_3)$_3$), 1.26 ppm (s, 36H, N(C(CH_3)$_3$). ^{13}C{^{1}H} NMR (150.90 MHz, C_6D_6, 298 K) δ = 146.3, 136.9, 132.1, 120.8, 119.6, 56.0, 35.9, 32.3, 31.8 ppm.

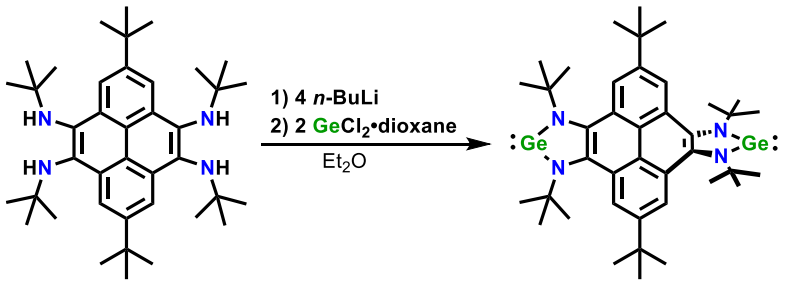

1 2

Synthesis of Compound 2. Compound **1** (1.00 g, 1.67 mmol) was dissolved in freshly distilled Et_2O (10 mL) in a 100 mL Schlenk flask to yield a yellow solution. *n*-BuLi (2.5 M in hexanes, 2.84 mL, 7.02 mmol) was added dropwise under argon at -78 °C, and a color change to red was observed. The reaction was slowly warmed to room temperature and stirred for 22 hrs. The solvent was removed under reduced pressure, and the orange residue was redissolved in toluene (60 mL). $GeCl_2$•dioxane (0.774 g, 3.34 mmol) was added, and the reaction was stirred for 17 hrs. The mixture was filtered over celite to leave a dark orange filtrate. The solvent was removed from the filtrate under reduced pressure to leave a dark orange solid. The crude solid was washed with hexane (3 x 10 mL) to leave the pure orange compound **2** (0.517 g, 46% yield). Yellow rod-shaped crystals suitable for X-ray diffraction studies were obtained from a concentrated toluene solution at -37 °C. ^{1}H NMR (600 MHz, C_6D_6, 298 K) δ = 8.50 (s, 4H, CH_{pyr}), 1.85 (s, 36H, N(C(CH_3)$_3$)) 1.59 ppm (s, 18H, C(CH_3)$_3$). ^{13}C{^{1}H} NMR (150.90 MHz, C_6D_6, 298 K) δ = 143.7, 136.8, 126.7, 117.2, 116.3, 59.3, 37.5, 36.4, 32.6 ppm. Anal. Calcd for $C_{40}H_{58}Ge_2H_4$: C, 64.91; H, 7.90; N, 7.57%. Found: C, 64.38; H, 8.14; N, 7.24%.

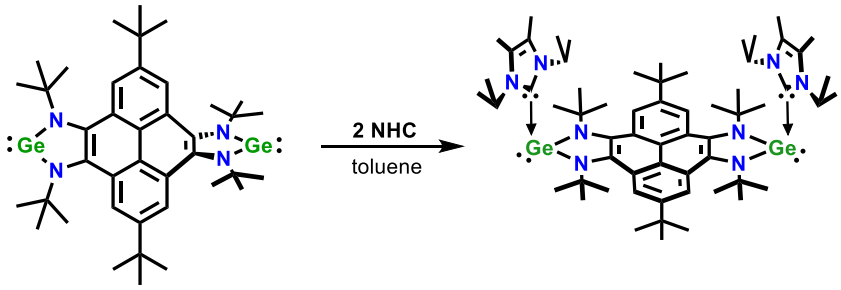

2 3

Synthesis of Compound 3. To a solution of compound **2** (0.200 g, 0.270 mmol) in toluene (25 mL), sIPr (0.0974 g, 0.540 mmol) was added. After addition, the reaction was stirred at room temperature for 3.5 hrs. The yellow precipitate was then collected through filtration and washed with hexane (3 x 5 mL), and the remaining solid was dried under reduced pressure to yield compound **3** (0.122 g, 41% yield). Yellow block-shaped crystals suitable for X-ray diffraction were obtained from a concentrated NMR sample in C_6D_6. ^{1}H NMR (600 MHz, C_6D_6, 298 K) δ = 8.57 (s, 4H, CH_{pyr}), 6.68 (br. s, 4H, CH(CH$_3$)$_2$), 1.99 (s, 36H, N(C(CH_3)$_3$)), 1.72 (s, 18H, C(CH_3)$_3$), 1.49 (s, 12H, CCH_3), 1.05 ppm (s, 24H, CH(CH_3)$_2$). ^{13}C{^{1}H} NMR (150.90 MHz, C_6D_6, 298 K) δ = 188.4, 141.9, 120.1, 119.3, 111.8, 58.4, 48.4, 36.2, 35.8, 33.0, 21.4, 9.8 ppm.

NMR Spectra: ^{1}H and ^{13}C NMR Spectra

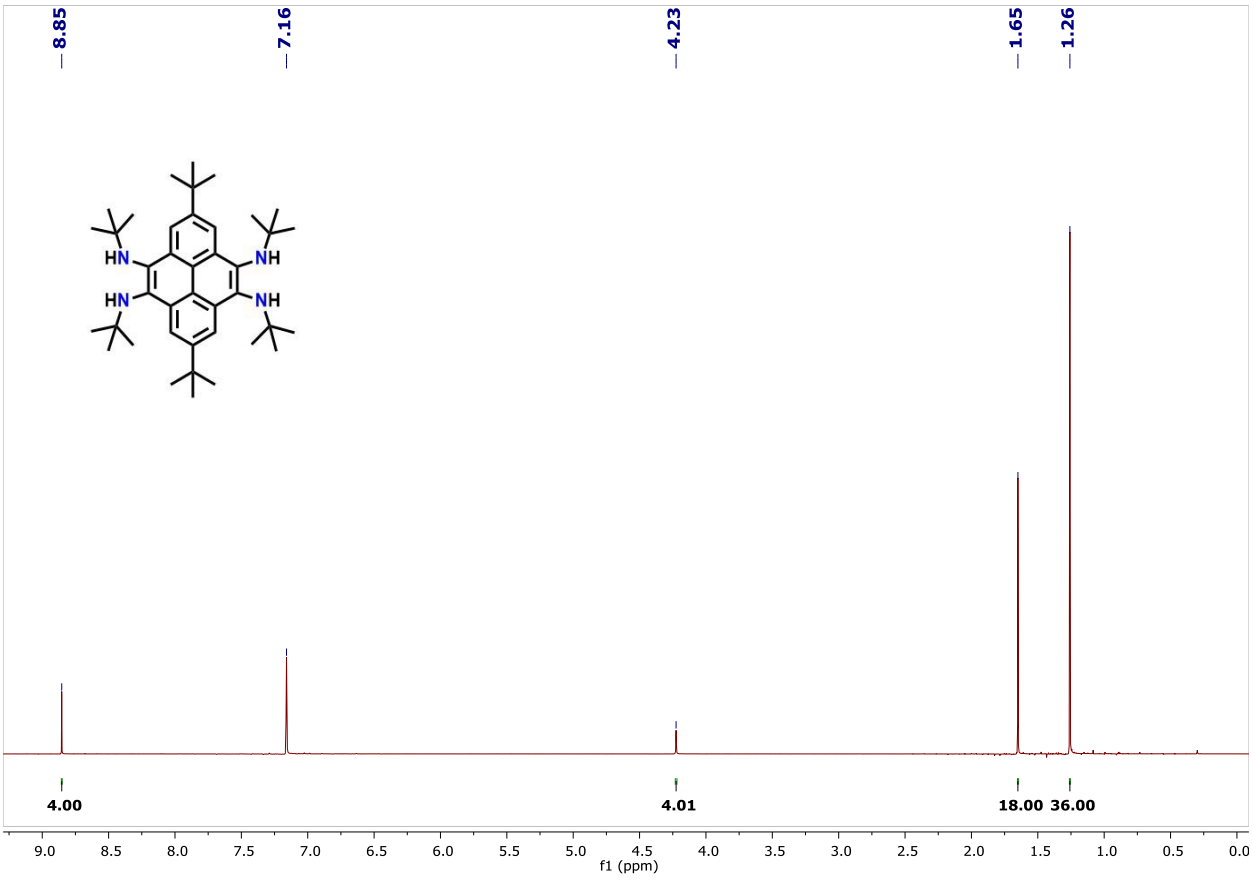

Figure S1. ^{1}H NMR spectrum (600 MHz, C_6D_6, 298 K) of **1**.

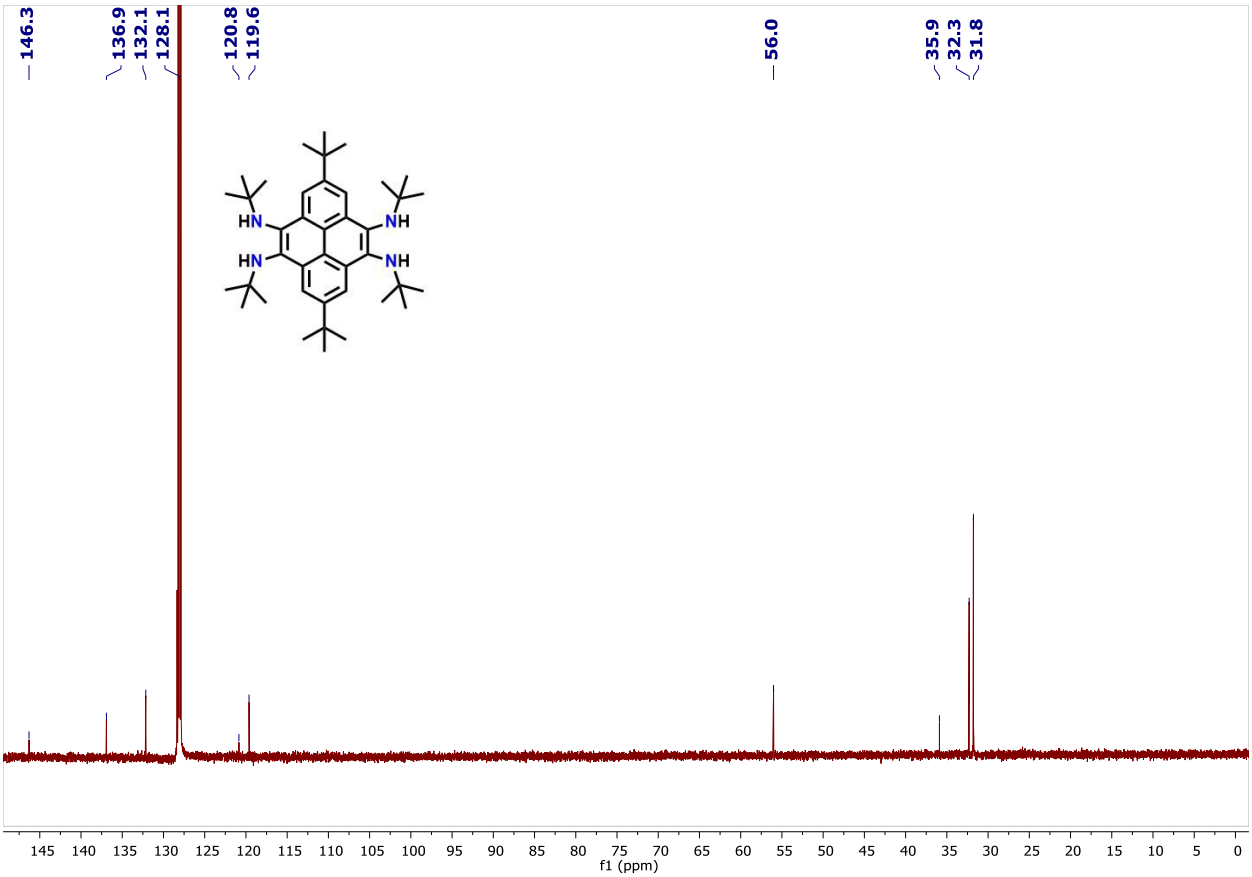

Figure S2. ^{13}C NMR spectrum (151 MHz, C_6D_6, 298 K) of **1**.

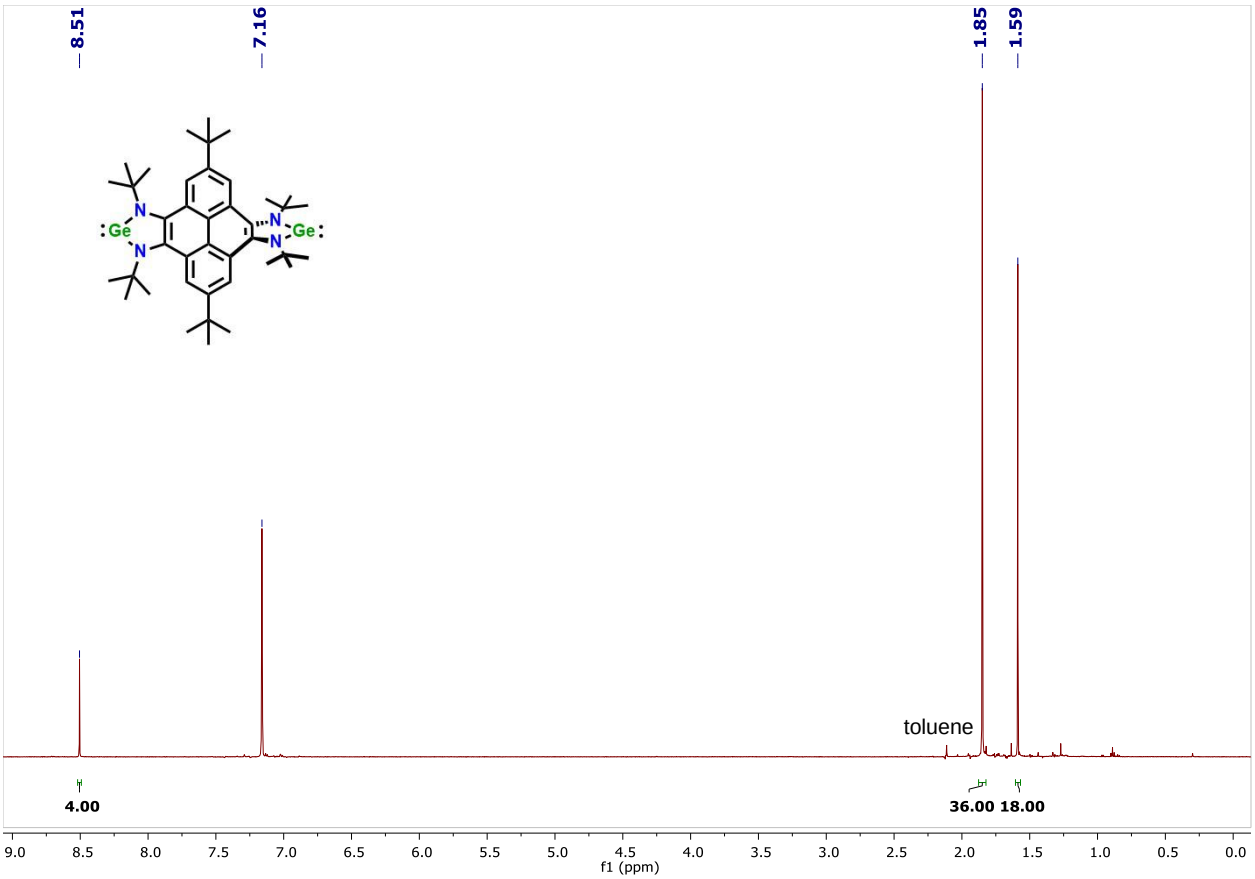

Figure S3. ^{1}H NMR spectrum (600 MHz, C_6D_6, 298 K) of **2**.

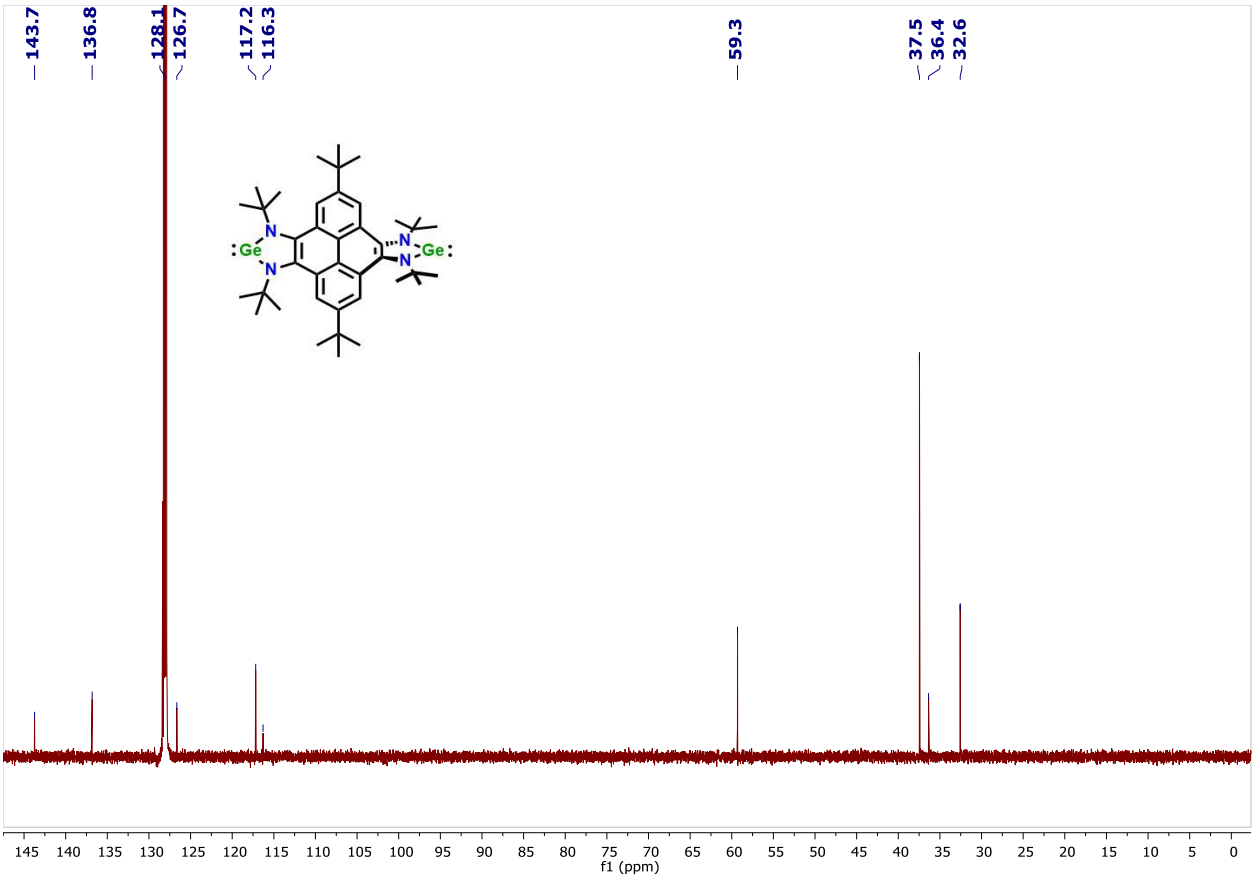

Figure S4. ^{13}C NMR spectrum (151 MHz, C_6D_6, 298 K) of **2**.

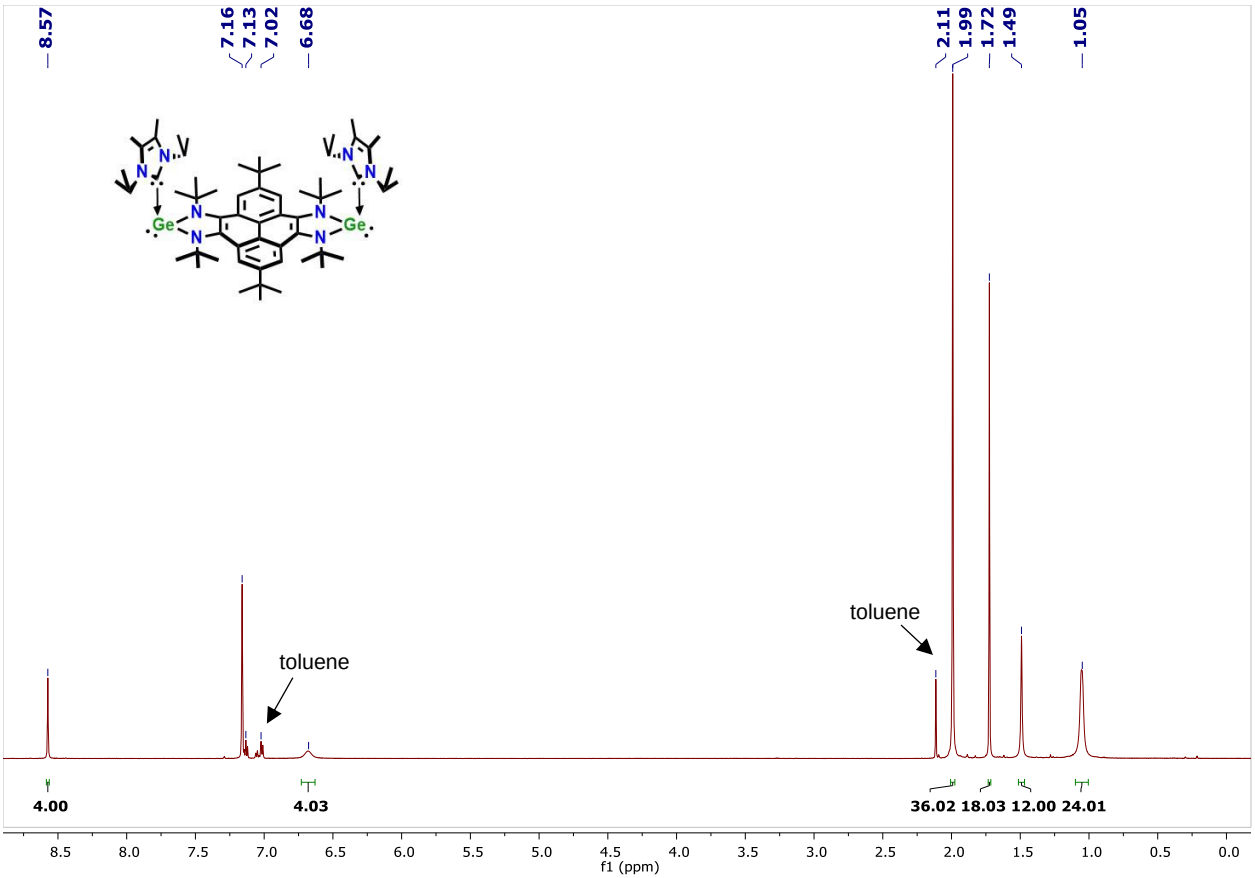

Figure S5. ^{1}H NMR spectrum (600 MHz, C_6D_6, 298 K) of **3**.

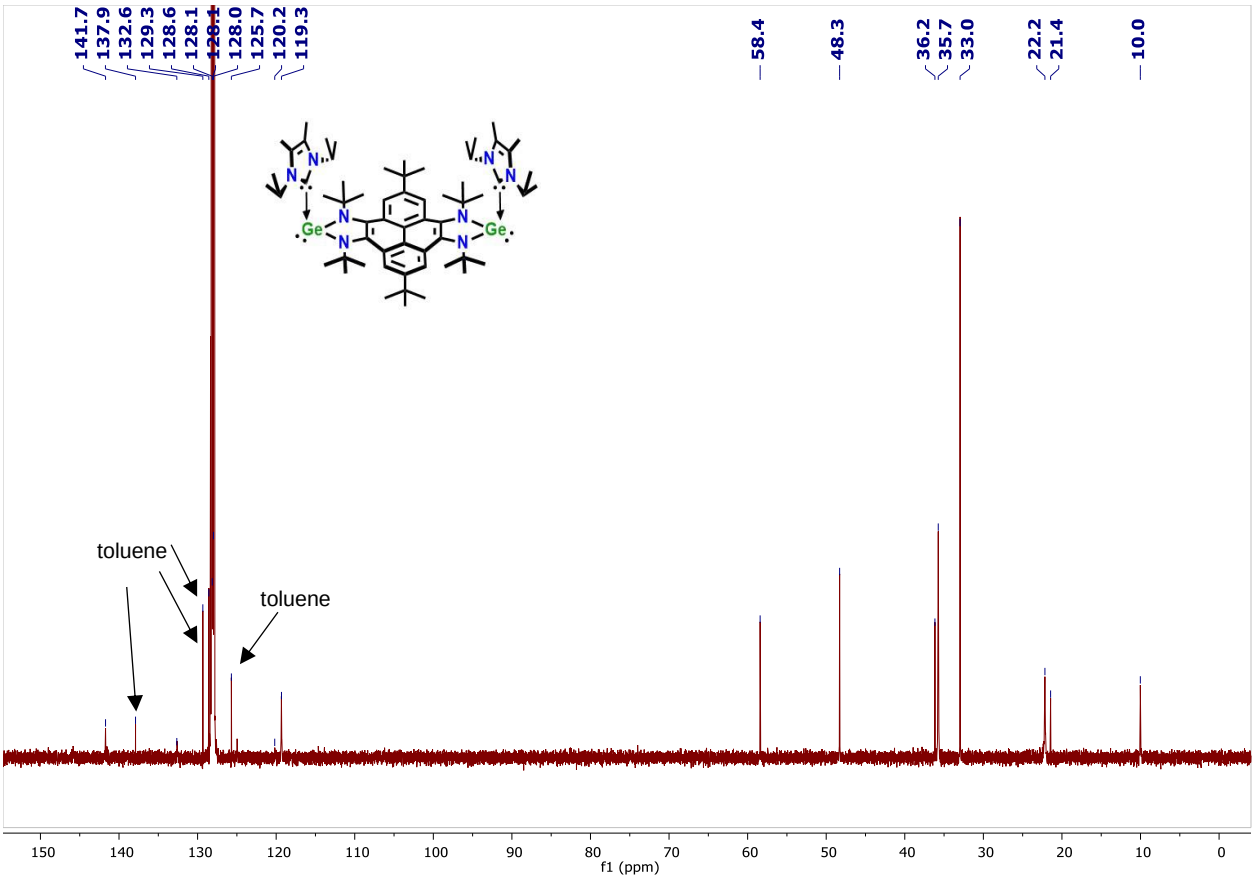

Figure S6. ^{13}C NMR spectrum (151 MHz, C_6D_6, 298 K) of **3**.

IR Spectra

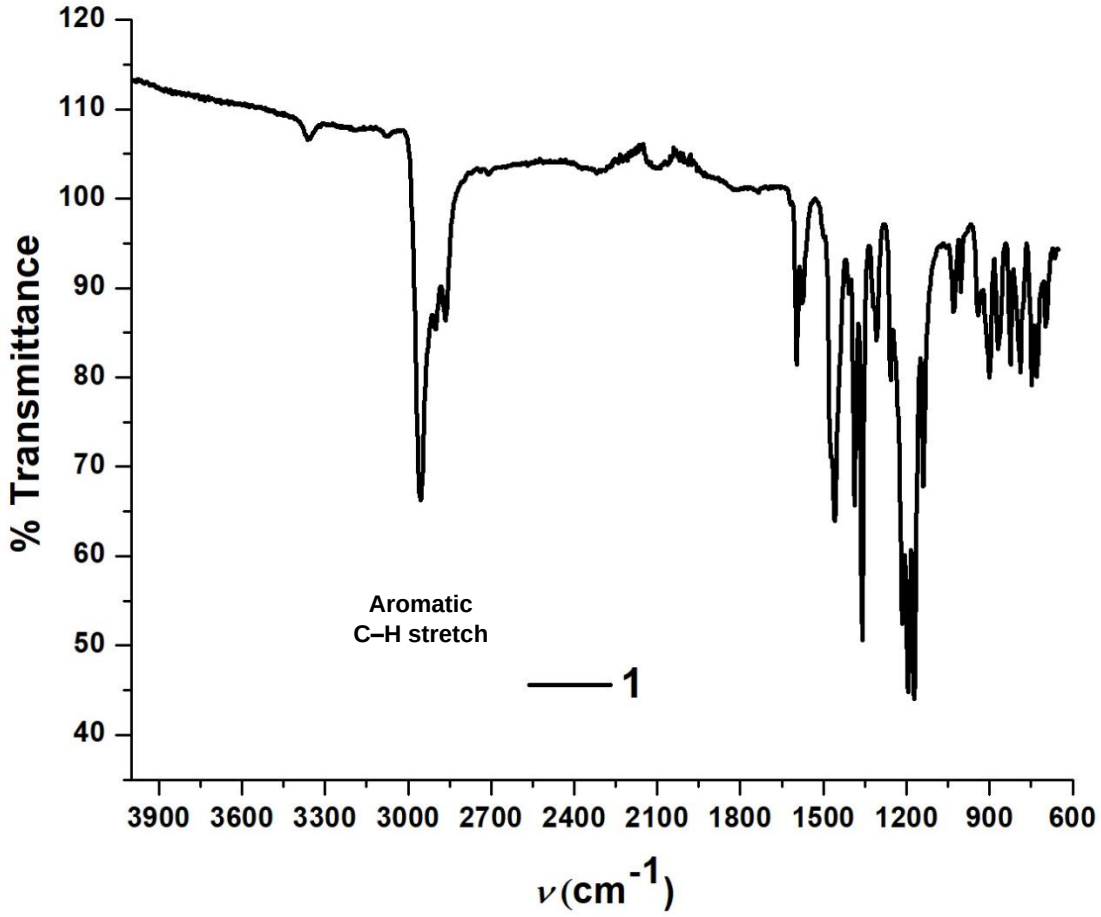

Figure S7. IR spectrum of compound **1**.

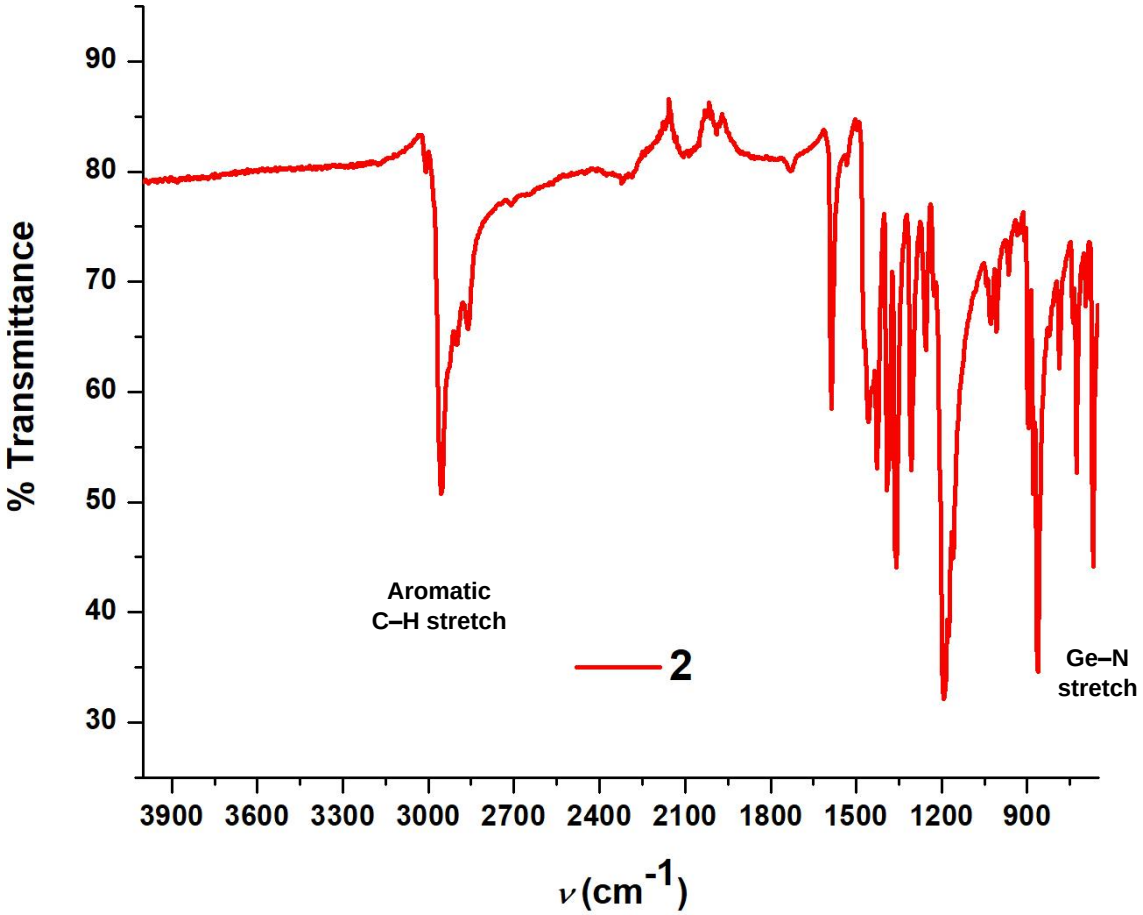

Figure S8. IR spectrum of compound **2**.

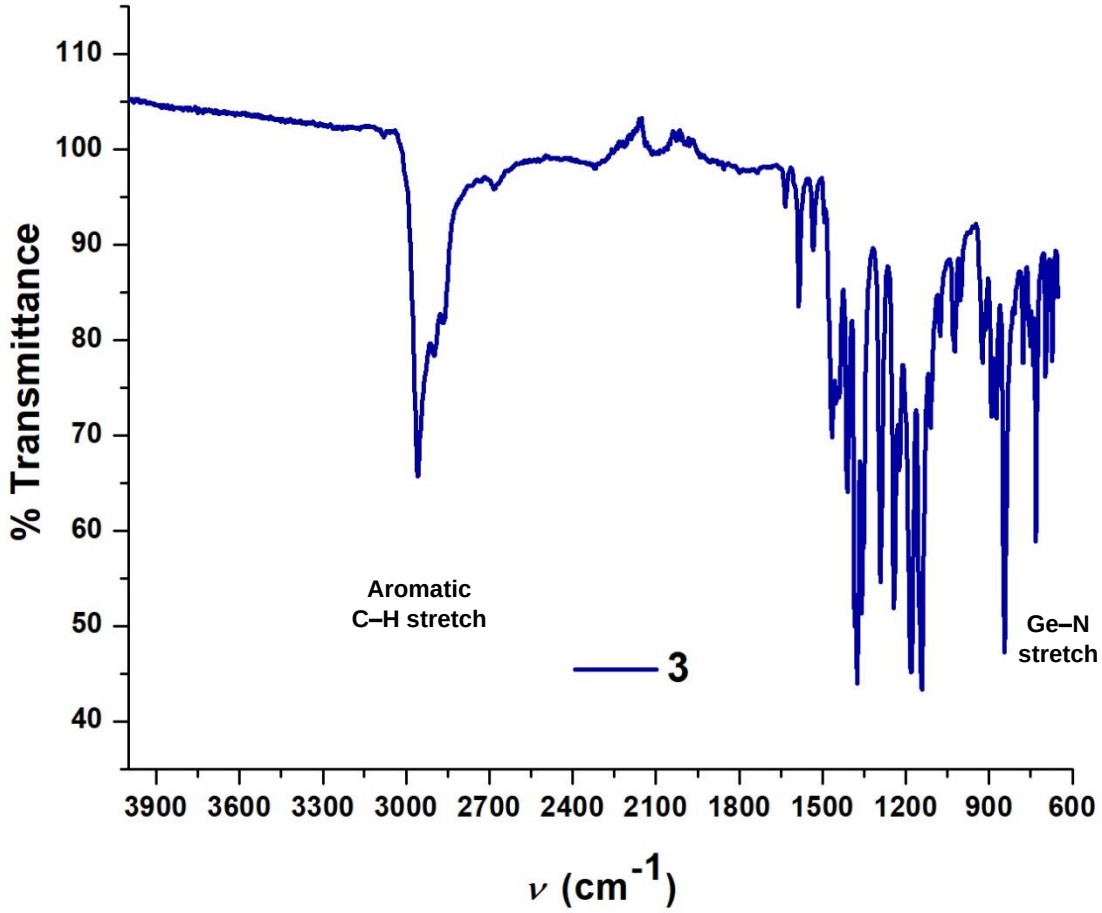

Figure S9. IR spectrum of compound **3**.

X-ray Crystallographic Data

Single crystals of **1**, **2**, or **3** were coated with Paratone oil and mounted on a MiTeGen MicroLoop. The X-ray intensity data were measured on a Bruker Kappa APEXII Duo diffractometer. Compound **1** was measured using an Incoatec Microfocus IμS (Cu K_α, λ = 1.54178 Å) and a multilayer mirror monochromator, and **2**, **3**, and **S4** used a fine-focus sealed tube (Mo K_α, λ = 0.71073 Å) and a graphite monochromator. The frames were integrated with the Bruker SAINT software package[4] using a narrow-frame algorithm. Data were corrected for absorption effects using the Multi-Scan method (SADABS).[4] The structures were solved and refined using the Bruker SHELXTL Software Package[5] within APEX3[4] and OLEX2.[6] Non-hydrogen atoms were refined anisotropically. The N-H hydrogen atoms in **1** were located in the diffraction map and refined isotropically. All other hydrogen atoms were placed in geometrically calculated positions with U_{iso} = 1.2U_{equiv} of the parent atom (U_{iso} = 1.5U_{equiv} for methyl). For **1**, two of *tert*-butyl groups and one N-H group were disordered over two positions, and one *tert*-butyl group was disordered over four positions. The relative occupancies of each disordered site were freely refined, and constraints were used on the anisotropic displacement parameters of the four-fold disordered *tert*-butyl. The symmetry disordered toluene solvent molecule was modeled at 50% occupancy. For **2**, two toluene solvent molecules that co-crystallized with the complex were well-behaved, but a third one was severely disordered and could not be successfully modeled with or without restraints. Thus, the structure factors were modified using the PLATON SQUEEZE[7] technique, in order to produce a "solvate-free" structure factor set. PLATON reported a total electron density of 53 e^- and total solvent accessible volume of 315 Å.[6] One tert-butyl group was found to be disordered over two positions. The relative occupancies were freely refined, and no constraints or restraints were used on the disordered atoms. For **3**, one benzene solvent molecule was disordered over two positions. The relative occupancy of the two positions was freely refined, and no constraints or restraints were needed on the disordered atoms. For the **S4**, the relative occupancy of each pair of disordered atoms was freely refined, with constraints on the anisotropic displacement parameters of all disordered atoms, and restraints on the bond lengths of minor *tert*-butyl components. Several molecules of severely disordered THF were present in the crystal but they could not be adequately modeled with or without restraints. Thus, the structure factors were modified using the PLATON SQUEEZE[7] technique, in order to produce a "solvate-free" structure factor set. PLATON reported a total electron density of 603 e^- and total solvent accessible volume of 1989 $Å^3$.

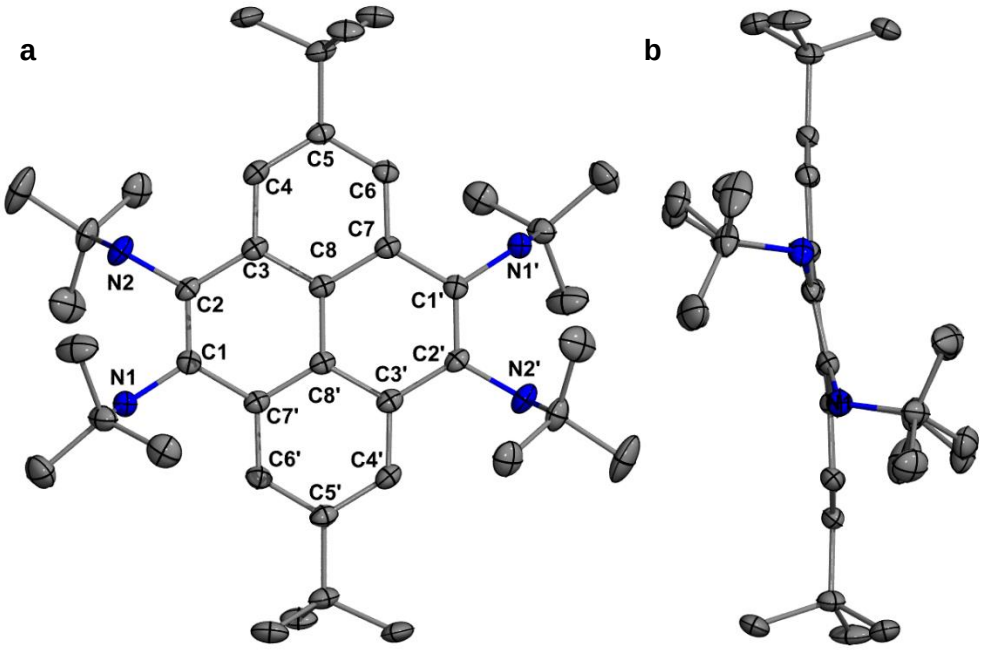

Figure S10. Crystal Structure of **1**. a) front view with atom labels, and b) side view displaying no twist angles. Thermal ellipsoids shown at 50% probability and H atoms were omitted for clarity. Twist angles (°): C2-C1-C2'-C1': 0; N2-N1-N2'-N1': 0.

Table S1. Crystal data for compounds **1**-**3** and **S4**.

	1	**2**	**3**	**S4**
Chemical formula	$C_{87}H_{132}N_8$	$C_{54}H_{74}Ge_2N_4$	$C_{86}H_{122}Ge_2N_8$	$C_{42.74}H_{66.23}Ge_2I_{1.26}N_4$
FW (g/mol)	1290.00	924.35	1413.09	940.89
Temperature (K)	100(2)	100(2)	100(2)	100(2)
Wavelength (Å)	1.54178	0.71073	0.71073	0.71073
Crystal size (mm)	0.131 x 0.132 x 0.148	0.074 x 0.102 x 0.228	0.161 x 0.167 x 0.214	0.294 x 0.314 x 0.438
Crystal habit	colorless block	yellow rod	yellow block	yellow block
Crystal system	triclinic	triclinic	monoclinic	orthorhombic
Space group	P -1	P -1	C 2/c	P n m a
a (Å)	11.1927(4)	11.7824(12)	16.5571(11)	19.7850(18)
b (Å)	13.6662(6)	13.8010(13)	17.5990(13)	17.7220(17)
c (Å)	13.8032(5)	16.8291(16)	27.336(2)	17.0451(16)
α (°)	108.458(2)	80.933(3)	90	90
β (°)	94.156(3)	77.324(3)	99.608(2)	90
γ (°)	96.504(2)	89.214(3)	90	90
Volume (Å^3)	1976.66(14)	2635.9(4)	7853.7(10)	5976.5(10)
Z	1	2	4	4
Calcd. Density (g/cm^3)	1.084	1.165	1.195	1.046
μ (mm^{-1})	0.470	1.176	0.814	
Theta range	3.40 to 68.34	1.26 to 25.71	1.70 to 28.32	1.58 to 25.40
Index ranges	-12 ≤ h ≤ 13 -16 ≤ k ≤ 16 -16 ≤ l ≤ 16	-12 ≤ h ≤ 14 -16 ≤ k ≤ 16 -20 ≤ l ≤ 20	-22 ≤ h ≤ 21 -23 ≤ k ≤ 23 -34 ≤ l ≤ 36	-23 ≤ h ≤ 23 -20 ≤ k ≤ 21 -20 ≤ l ≤ 20
Reflections collected	28562	42614	47450	47710
Independent reflections	7244 [R_{int} = 0.0530]	10041 [R_{int} = 0.0828]	9759 [R_{int} = 0.0578]	5677 [R_{int} = 0.0517]
Data / restraints / parameters	7244 / 1 / 589	10041 / 0 / 592	9759 / 0 / 477	5677 / 6 / 2252
Goodness-of-fit on F²	1.043	1.019	1.008	1.052
R1 I>2σ(I)	0.0463	0.0468	0.0365	0.1012
wR2 (all data)	0.1261	0.1143	0.0804	0.2220
CCDC number	1946973	1946974	1946975	1962780

Reaction of 2 with Methyl Iodide

To address a reviewer comment regarding whether or not the twisting of compound **2** was due to a steric or electronic effect, we reacted **2** with MeI to obtain a compound containing two Ge(IV) centers. After heating a mixture of **2** and MeI to 50 °C in THF for 16 hrs the solvent was removed. Proton NMR of the solid indicated a complex mixture containing several products. Single crystals from six different batches were grown from a concentrated THF solution at -37 °C. In each case the structure distinctly revealed Ge(IV) centers with different ratios of Me and I (Figure S11). In all cases the structures contain a bent pyrene core and therefore we attribute the extremely twisted structure of **2** to be due to the steric interaction of the *N*-(*tert*-butyl) groups and the pyrene-H.

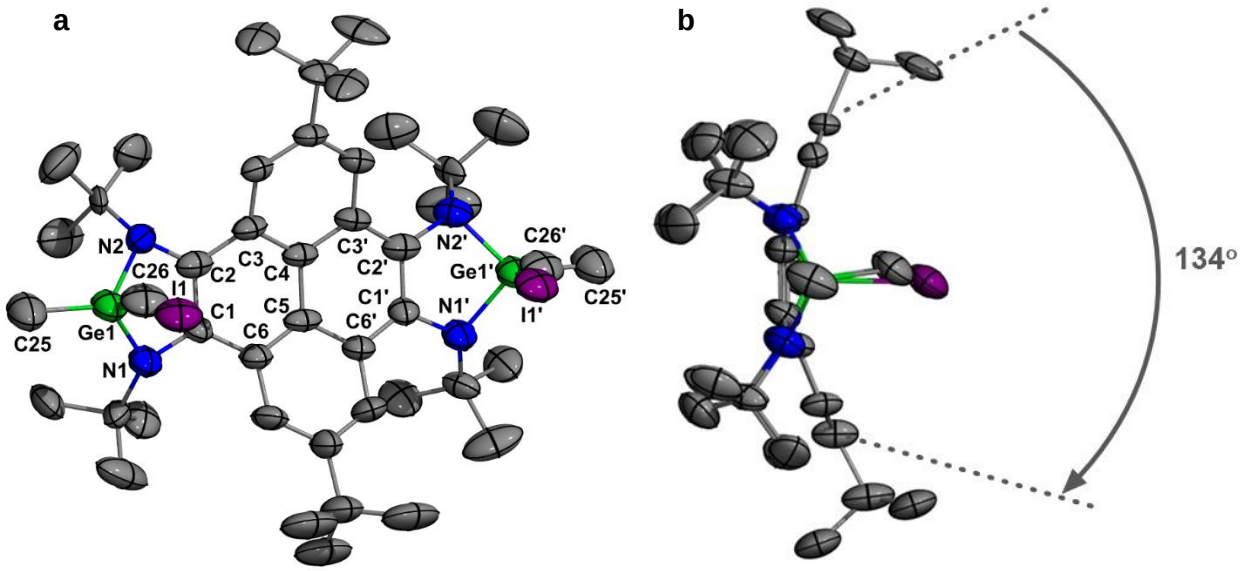

Figure S11. Crystal Structure of **S4**. a) Front view with atom labels, and b) side view displaying bend angle. Thermal ellipsoids shown at 50% probability and H atoms were omitted for clarity. The structure is a mixture of methyl iodide to dimethyl where the occupancy of the I atom is 60%, and the remaining 40% corresponds to Me. Bend angle (°): 134. The bend angle refers to the angle between the torsion planes containing the C7-C8-C7', and C9-C10-C9' atoms.

Theoretical Calculations

The starting geometries of compounds **2** and **3** were extracted from the X-ray crystal structures. Hydrogen positions were optimized using the Universal Force Field (UFF) freezing the location of all other atoms. The geometry of structure of **1** was generated from the molecular geometry of compound **2** from the X-ray crystal structure (the valency of the four amine nitrogens were satisfied with hydrogen atoms) and subsequently optimizing the structure at the B3LYP/BS1 level of theory. The DFT-optimized geometry of compound **2** (structure **2^a**, the lowest energy conformer) compares quite favorably with molecular geometry from the X-ray crystal structure. All subsequent electronic structure theory computations were carried out as single-point computations on these geometries. All computations were carried out using Gaussian 16 Revision B.01.[8] The basis sets used were BS1 (BS1 = 6-31G(d') basis set[9-11] for C, H, and N; LANL2DZ(d,p) with LANL2DZ ECP for Ge)[12,13] and BS2 (BS2 = 6-311+G** basis sets[14,15] for C, H, and N; 6-311G** basis set[16] for Ge). Nucleus-Independent Chemical Shift (NICS) values[17] were computed for each aromatic ring of the compounds by computing gas phase magnetic shielding tensors of ghost atoms placed at the centroid of each ring [NICS(0)] using the Gauge Independent Atomic Orbital (GIAO)[18-21] method at the B3LYP/BS2 level of theory.[22,23] To simulate the absorption spectra, the first twenty vertical transitions were computed with B3LYP/BS1 using time dependent density functional theory (TD-DFT).[24] Simulated absorption spectra were obtained using an in-house Fortran program by convoluting the computed excitation energies and oscillator strengths with a Gaussian line-shape and a broadening of 20 nm. Orbital pictures were generated using Chemcraft with a contour value of 0.05. Structural comparisons and overlay figures were generated with JIMP2.[25-27]

Frontier Molecular Orbitals

MO 166 LUMO –0.03729 Ha

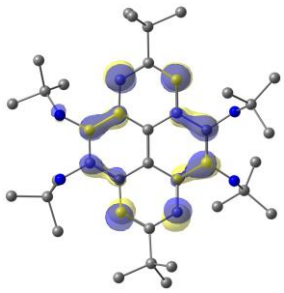

MO 165 HOMO –0.16233 Ha

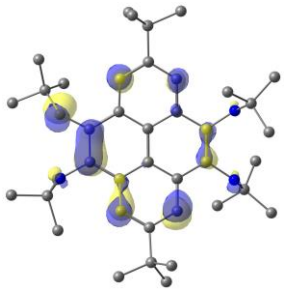

Figure S12. Selected frontier molecular orbitals for the DFT-optimized geometry of compound **1** and their energies in Hartrees (Ha).

MO 168 LUMO –0.03933 Ha

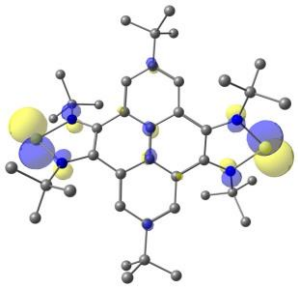

MO 167 HOMO –0.15373 Ha

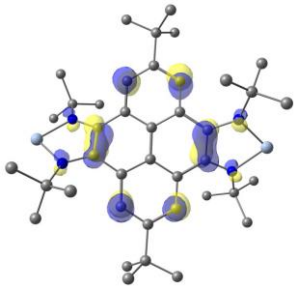

MO 163 HOMO – 4 –0.23229 Ha

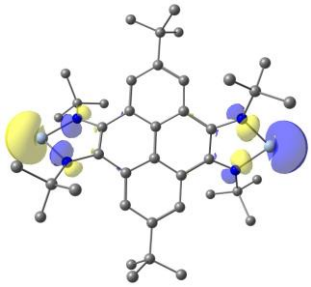

MO 162 HOMO – 5 –0.23563 Ha

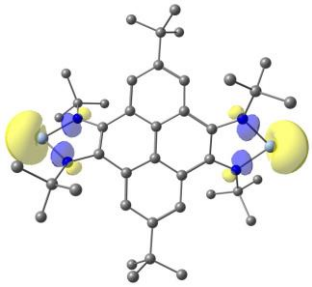

Figure S13. Selected frontier molecular orbitals for the DFT-optimized geometry of compound **2[a]** and their energies in Hartrees (Ha).

MO 268 LUMO –0.01988 Ha

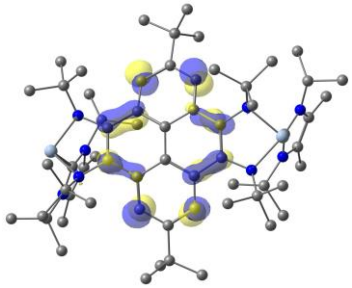

MO 267 HOMO –0.13473 Ha

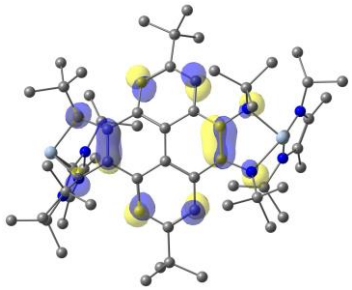

MO 265 HOMO – 2 –0.16555 Ha

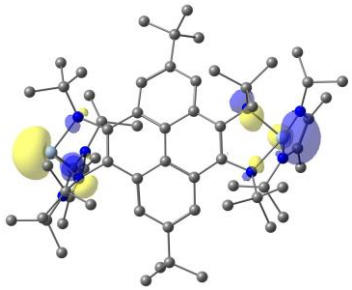

MO 264 HOMO – 3 –0.16776 Ha

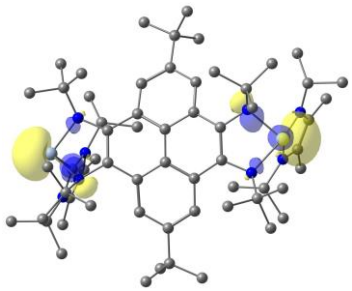

Figure S14. Selected frontier molecular orbitals for the DFT-optimized geometry of compound **3**[a] and their energies in Hartrees (Ha).

Simulated UV-vis Spectra

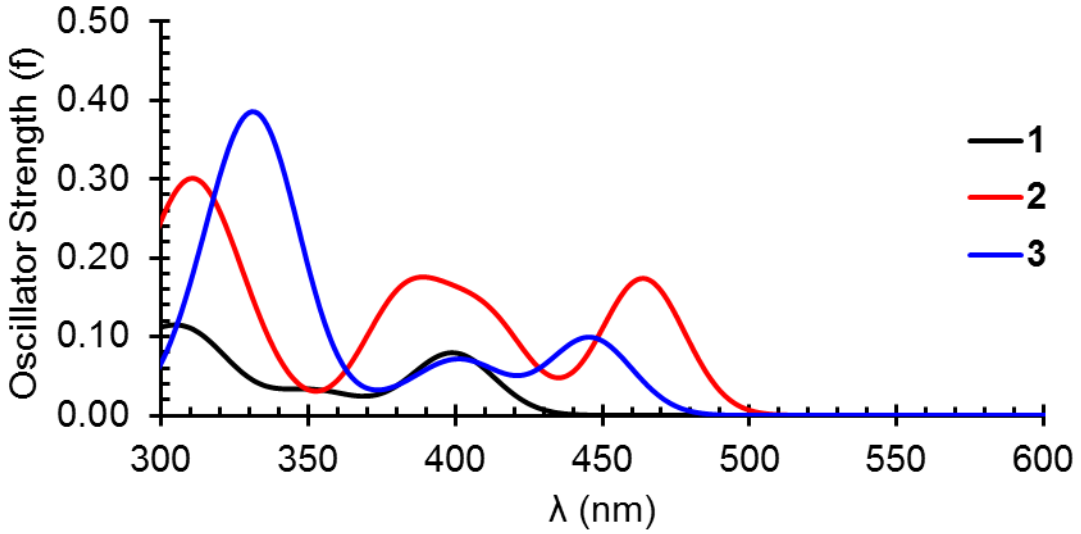

Figure S15. Simulated UV-vis absorption spectra of **1-3**. The above spectrum shows simulated UV-vis for **1**, **2**[a], and **3**[a]. The λ_{max} of **1** is very similar in wavelength to the shoulder peak of **3** (399 nm and 404 nm, respectively). The λ_{max} of **2**[a] is more red shifted than the λ_{max} of both **1** and **3**[a].

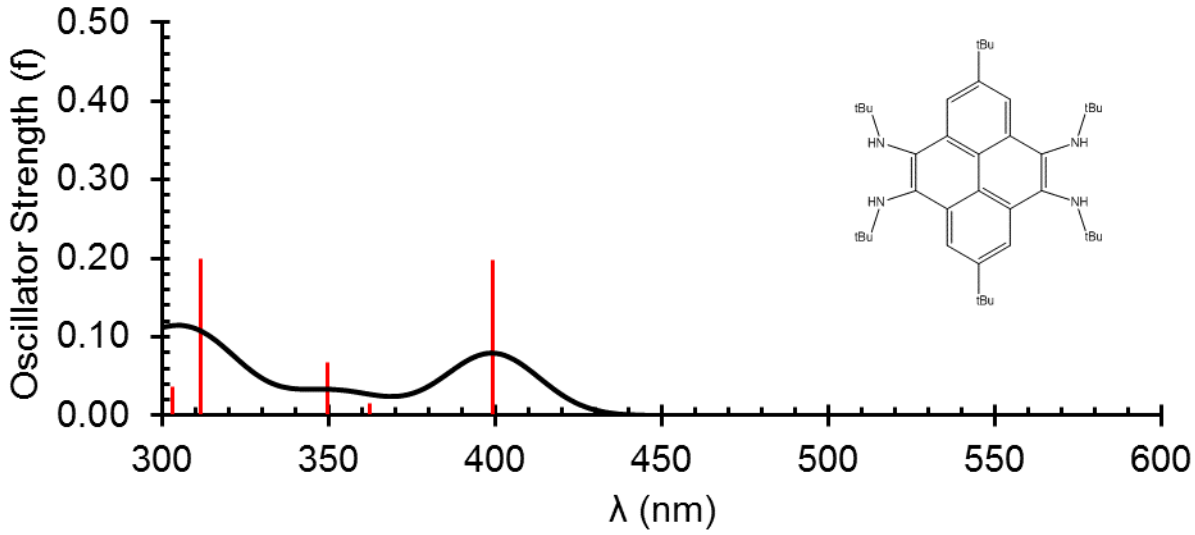

Figure S16. Simulated UV-vis absorption spectrum from TDDFT excitations for compound **1**.

Table S2. Electronic transitions for the calculated transitions of **1** and their orbital contributions.

λ (nm)	Character	% NTO Contribution
399	$\pi \rightarrow \pi^*$	96%
350	$\pi \rightarrow \pi^*$	90%
312	$\pi \rightarrow \pi^*$	59%
	$\pi \rightarrow \pi^*$	37%

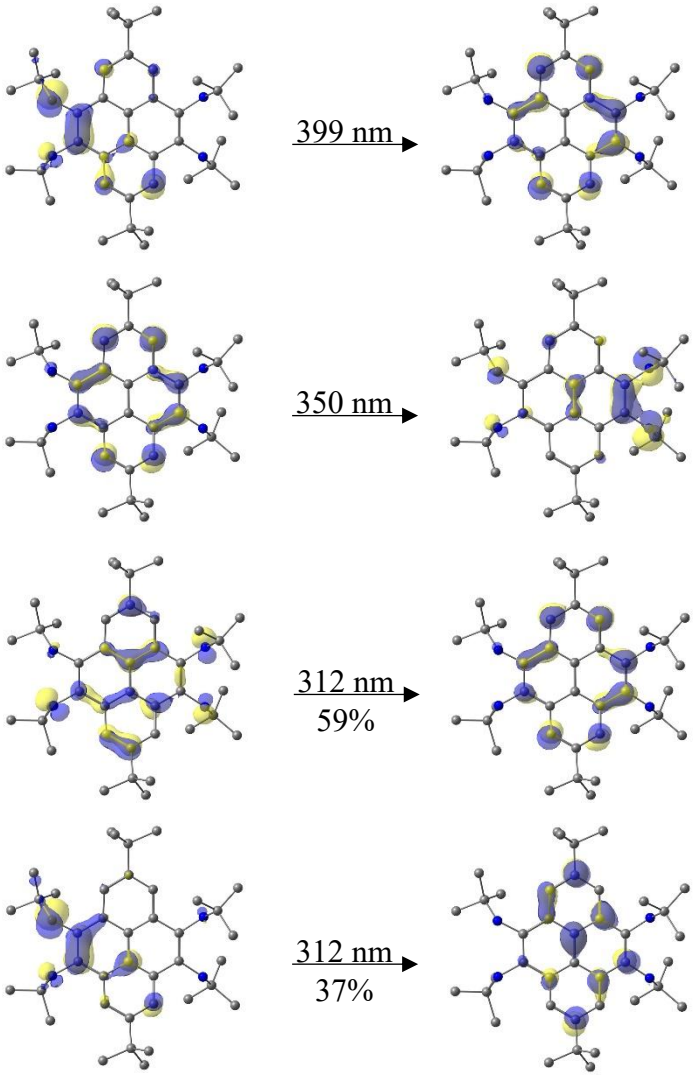

Figure S17. Natural Transition Orbitals (NTO) for the calculated transitions of **1**.

Output for TDDFT excitations for compound 1

```
HOMO is 165

 ES with f > 0.01

Excited State 1: Singlet-A 3.1058 eV 399.21 nm 0.1968 <S**2>=0.000
Excited State 2: Singlet-A 3.4204 eV 362.49 nm 0.0148 <S**2>=0.000
Excited State 3: Singlet-A 3.5437 eV 349.88 nm 0.0677 <S**2>=0.000
Excited State 4: Singlet-A 3.9802 eV 311.50 nm 0.1996 <S**2>=0.000
Excited State 5: Singlet-A 4.0915 eV 303.03 nm 0.0361 <S**2>=0.000
Excited State 6: Singlet-A 4.2730 eV 290.16 nm 0.1047 <S**2>=0.000
Excited State 8: Singlet-A 4.4183 eV 280.62 nm 0.0163 <S**2>=0.000
Excited State 9: Singlet-A 4.6835 eV 264.72 nm 0.0474 <S**2>=0.000
Excited State 10: Singlet-A 4.6921 eV 264.24 nm 0.0373 <S**2>=0.000
Excited State 11: Singlet-A 4.7965 eV 258.49 nm 0.0712 <S**2>=0.000
Excited State 12: Singlet-A 5.0209 eV 246.94 nm 0.4341 <S**2>=0.000
Excited State 14: Singlet-A 5.1493 eV 240.78 nm 0.1031 <S**2>=0.000
Excited State 15: Singlet-A 5.1907 eV 238.86 nm 0.1105 <S**2>=0.000
Excited State 16: Singlet-A 5.2168 eV 237.66 nm 0.0400 <S**2>=0.000
Excited State 17: Singlet-A 5.3219 eV 232.97 nm 0.2195 <S**2>=0.000
Excited State 18: Singlet-A 5.3564 eV 231.47 nm 0.0196 <S**2>=0.000
Excited State 19: Singlet-A 5.4745 eV 226.47 nm 0.2745 <S**2>=0.000

 Excited State   1:      Singlet-A      3.1058 eV  399.21 nm  0.1968  <S**2>=0.000
     163 ->167         0.10976
     164 ->166         0.18117
     165 ->166         0.66529

 Excited State   2:      Singlet-A      3.4204 eV  362.49 nm  0.0148  <S**2>=0.000
     163 ->166        -0.31092
     164 ->166         0.26769
     165 ->167         0.56513

 Excited State   3:      Singlet-A      3.5437 eV  349.88 nm  0.0677  <S**2>=0.000
     163 ->166         0.21797
     164 ->166         0.61442
     165 ->166        -0.13819
     165 ->167        -0.19637

 Excited State   4:      Singlet-A      3.9802 eV  311.50 nm  0.1996  <S**2>=0.000
     161 ->166         0.12628
     163 ->166         0.51186
     164 ->167         0.24665
     165 ->167         0.32611
     165 ->168        -0.15490

 Excited State   5:      Singlet-A      4.0915 eV  303.03 nm  0.0361  <S**2>=0.000
     163 ->166         0.10538
     165 ->168         0.67430

 Excited State   6:      Singlet-A      4.2730 eV  290.16 nm  0.1047  <S**2>=0.000
     160 ->166         0.10046
     162 ->166        -0.12630
     163 ->166        -0.21391
     163 ->168         0.11001
     164 ->167         0.61440

 Excited State   8:      Singlet-A      4.4183 eV  280.62 nm  0.0163  <S**2>=0.000
     161 ->166         0.63521
     163 ->167        -0.13486
     165 ->169        -0.17218

 Excited State   9:      Singlet-A      4.6835 eV  264.72 nm  0.0474  <S**2>=0.000
     160 ->166         0.43921
     163 ->167        -0.29525
     165 ->169        -0.39108

 Excited State  10:      Singlet-A      4.6921 eV  264.24 nm  0.0373  <S**2>=0.000
     159 ->166         0.16359
     160 ->166         0.42049
```

```
    161 ->166         0.14810
    163 ->167        -0.13675
    165 ->169         0.47233

Excited State  11:      Singlet-A      4.7965 eV  258.49 nm  0.0712  <S**2>=0.000
    160 ->166        -0.25110
    161 ->167        -0.10452
    163 ->167        -0.38864
    164 ->168         0.48384

Excited State  12:      Singlet-A      5.0209 eV  246.94 nm  0.4341  <S**2>=0.000
    160 ->166         0.10523
    160 ->167        -0.14007
    161 ->166         0.12780
    161 ->167         0.24031
    163 ->167         0.34616
    163 ->168        -0.17960
    164 ->168         0.44059

Excited State  14:      Singlet-A      5.1493 eV  240.78 nm  0.1031  <S**2>=0.000
    158 ->166         0.16162
    159 ->166         0.39917
    159 ->167        -0.11303
    160 ->166        -0.10661
    161 ->167         0.15928
    162 ->167         0.22047
    163 ->167        -0.11130
    163 ->168        -0.35844
    164 ->169        -0.17832

Excited State  15:      Singlet-A      5.1907 eV  238.86 nm  0.1105  <S**2>=0.000
    159 ->166         0.26724
    161 ->167         0.14115
    162 ->167         0.24601
    163 ->168         0.50698
    164 ->168         0.10538
    164 ->169        -0.15318

Excited State  16:      Singlet-A      5.2168 eV  237.66 nm  0.0400  <S**2>=0.000
    158 ->166         0.16744
    159 ->166         0.16213
    161 ->167        -0.39266
    162 ->167         0.21079
    164 ->169         0.44372

Excited State  17:      Singlet-A      5.3219 eV  232.97 nm  0.2195  <S**2>=0.000
    158 ->166         0.19924
    159 ->166        -0.25110
    161 ->167         0.33648
    162 ->167         0.15553
    162 ->168        -0.14050
    163 ->167        -0.13769
    163 ->169        -0.18458
    164 ->169         0.27053
    165 ->169         0.12876
    165 ->170        -0.13889
    165 ->171        -0.15128

Excited State  18:      Singlet-A      5.3564 eV  231.47 nm  0.0196  <S**2>=0.000
    158 ->166         0.12140
    164 ->170        -0.14663
    165 ->170         0.65388

Excited State  19:      Singlet-A      5.4745 eV  226.47 nm  0.2745  <S**2>=0.000
    158 ->166         0.33708
    159 ->166        -0.18228
    160 ->167         0.13266
    161 ->167        -0.26499
    163 ->167         0.10321
    163 ->169        -0.15887
    164 ->169        -0.30850
    165 ->171        -0.22431
```

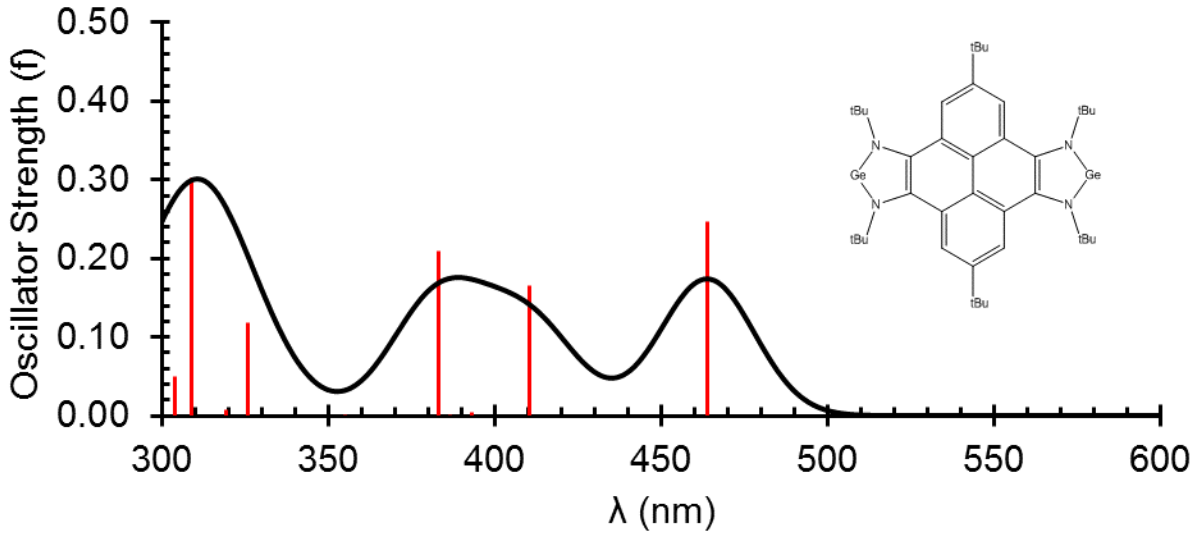

Figure S18. Simulated UV-vis absorption spectrum from TDDFT excitations for compound **2**[a].

Table S3. Electronic transitions for the calculated transitions of **2**[a] and their orbital contributions.

λ (nm)	Character	% NTO Contribution
464	$\pi \rightarrow$ Ge $p + \pi^*$	98%
411	$\pi \rightarrow \pi^*$	92%
383	$\pi \rightarrow$ Ge $p + \pi^*$	99%
309	$\pi \rightarrow \pi^*$	52%
	$\pi \rightarrow \pi^*$	41%

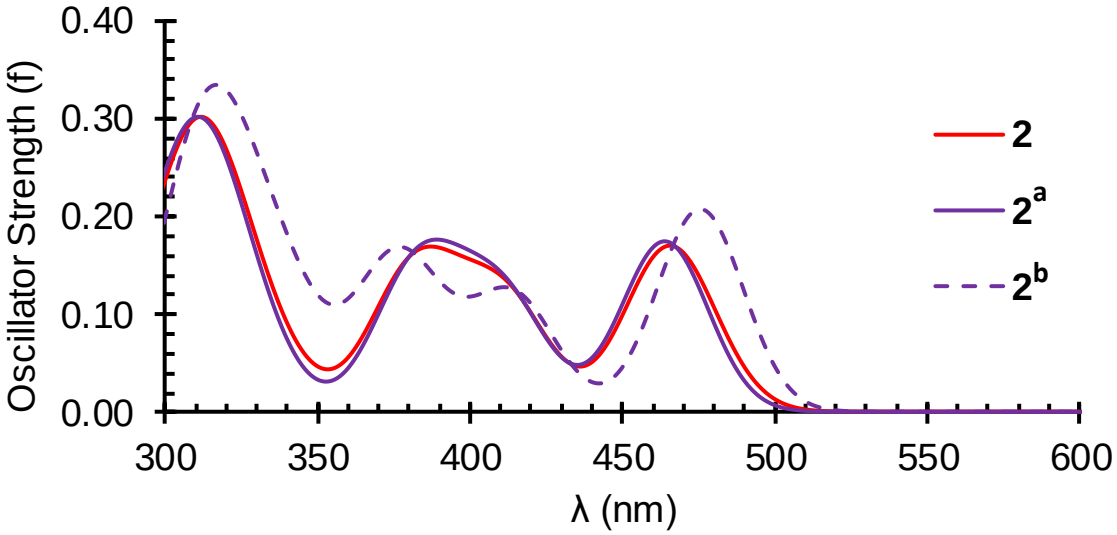

Figure S19. Spectral overlay for **2**, comprised of **2**[a] and **2**[b], in which **2** is the weighted average simulated spectrum of **2**[a] and **2**[b] (**2**[a] and **2**[b] are low energy structures of **2**).

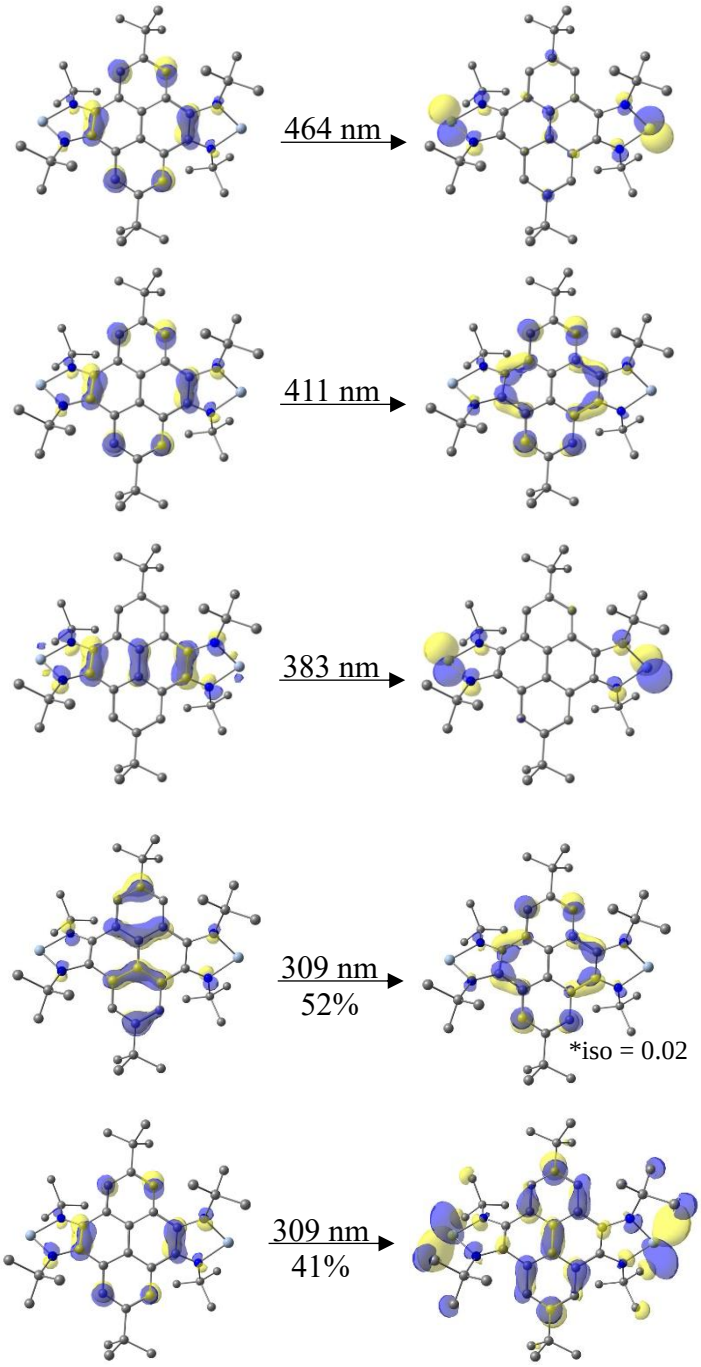

Figure S20. Natural Transition Orbitals (NTO) for the calculated transitions of **2**[a].

Output for TDDFT excitations for compound 2[a]

```
HOMO is 167

 ES with f > 0.01

Excited State 1: Singlet-A 2.6724 eV 463.94 nm 0.2463 <S**2>=0.000
Excited State 3: Singlet-A 3.0202 eV 410.51 nm 0.1660 <S**2>=0.000
Excited State 6: Singlet-A 3.2364 eV 383.10 nm 0.2088 <S**2>=0.000
Excited State 9: Singlet-A 3.8057 eV 325.79 nm 0.1175 <S**2>=0.000
Excited State 12: Singlet-A 4.0125 eV 309.00 nm 0.3017 <S**2>=0.000
Excited State 14: Singlet-A 4.0813 eV 303.79 nm 0.0506 <S**2>=0.000
Excited State 18: Singlet-A 4.4408 eV 279.19 nm 0.0465 <S**2>=0.000
Excited State 20: Singlet-A 4.4737 eV 277.14 nm 0.0118 <S**2>=0.000

 Excited State   1:      Singlet-A      2.6724 eV  463.94 nm  0.2463  <S**2>=0.000
     167 ->168         0.70098

 Excited State   3:      Singlet-A      3.0202 eV  410.51 nm  0.1660  <S**2>=0.000
     165 ->168         0.15969
     167 ->170         0.67799

 Excited State   6:      Singlet-A      3.2364 eV  383.10 nm  0.2088  <S**2>=0.000
     166 ->169         0.70267

 Excited State   9:      Singlet-A      3.8057 eV  325.79 nm  0.1175  <S**2>=0.000
     165 ->168         0.66981
     167 ->170        -0.13868

 Excited State  12:      Singlet-A      4.0125 eV  309.00 nm  0.3017  <S**2>=0.000
     165 ->170         0.50746
     167 ->171        -0.28504
     167 ->174        -0.34784

 Excited State  14:      Singlet-A      4.0813 eV  303.79 nm  0.0506  <S**2>=0.000
     165 ->170         0.30890
     166 ->172         0.13547
     166 ->173         0.11972
     167 ->171        -0.16560
     167 ->174         0.56747

 Excited State  18:      Singlet-A      4.4408 eV  279.19 nm  0.0465  <S**2>=0.000
     160 ->168        -0.10646
     163 ->168         0.15378
     164 ->169         0.42484
     165 ->168        -0.11946
     165 ->171        -0.14776
     166 ->172        -0.29580
     166 ->173         0.36737

 Excited State  20:      Singlet-A      4.4737 eV  277.14 nm  0.0118  <S**2>=0.000
     164 ->168         0.67393
```

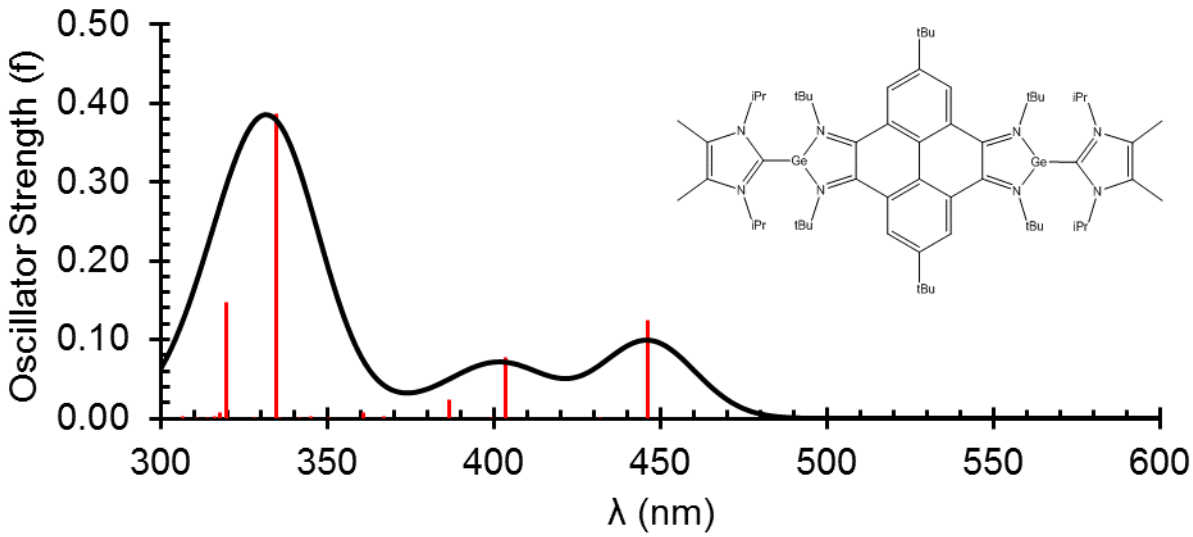

Figure S21. Simulated UV-vis absorption spectrum from TDDFT excitations for compound **3[a]**.

Table S4. Electronic transitions for the calculated transitions of **3[a]** and their orbital contributions.

λ (nm)	Character	% NTO Contribution
446	$\pi \rightarrow \pi^*$	96%
404	$\pi \rightarrow \pi^*$	87%
335	$\pi \rightarrow \pi^*$	81%

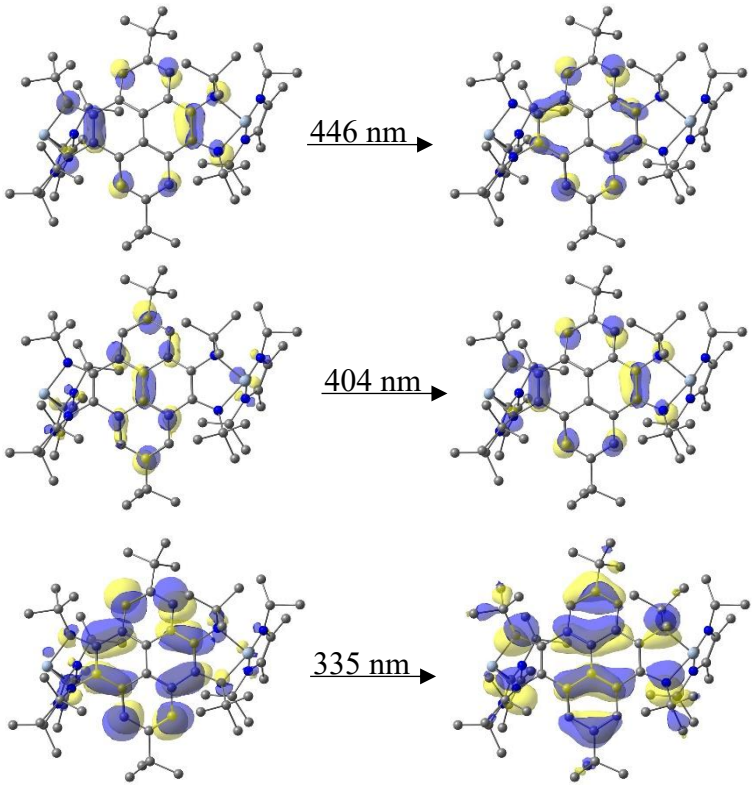

Figure S22. Natural Transition Orbitals (NTO) for the calculated transitions of **3**[a].

Output for TDDFT excitations for compound 3[a]

```
HOMO is 267

 ES with f > 0.01

Excited State 1: Singlet-A 2.7802 eV 445.96 nm 0.1253 <S**2>=0.000
Excited State 3: Singlet-A 3.0722 eV 403.57 nm 0.0775 <S**2>=0.000
Excited State 5: Singlet-A 3.2074 eV 386.55 nm 0.0232 <S**2>=0.000
Excited State 12: Singlet-A 3.7042 eV 334.71 nm 0.3859 <S**2>=0.000
Excited State 15: Singlet-A 3.8800 eV 319.55 nm 0.1472 <S**2>=0.000

 Excited State   1:      Singlet-A      2.7802 eV  445.96 nm  0.1253  <S**2>=0.000
     267 -> 268        0.68224

 Excited State   3:      Singlet-A      3.0722 eV  403.57 nm  0.0775  <S**2>=0.000
     263 -> 268        0.19711
     266 -> 269       -0.12537
     267 -> 270        0.62347
     267 -> 271       -0.21467

 Excited State   5:      Singlet-A      3.2074 eV  386.55 nm  0.0232  <S**2>=0.000
     263 -> 268       -0.14752
     266 -> 269       -0.25054
     267 -> 268        0.10456
     267 -> 270        0.19795
     267 -> 271        0.59571

 Excited State  12:      Singlet-A      3.7042 eV  334.71 nm  0.3859  <S**2>=0.000
     263 -> 268        0.63056
     267 -> 270       -0.11125
     267 -> 271        0.19929

 Excited State  15:      Singlet-A      3.8800 eV  319.55 nm  0.1472  <S**2>=0.000
     262 -> 268       -0.17992
     264 -> 270        0.37277
     264 -> 271        0.18752
     265 -> 269        0.51094
```

Nucleus Independent Chemical Shifts

NICS(0) values (B3LYP/BS2):

	1
Bq^2	–3.89
Bq^3	–10.66
Bq^4	–3.95
Bq^5	–10.45

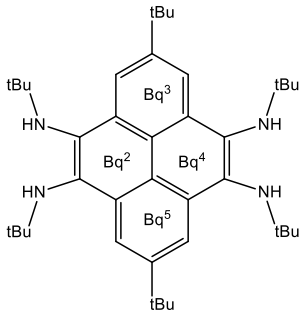

Figure S23. NICS(0) values for **1**.

	2	**2[a]**	**2-H**
Bq^1	–5.90	–5.85	–7.91
Bq^2	–3.66	–3.02	–4.91
Bq^3	–9.98	–10.11	–11.52
Bq^4	–2.86	–3.74	–4.92
Bq^5	–9.99	–10.11	–11.52
Bq^6	–5.83	–5.84	–7.91

(Expt) and computed distances of Ge-N bond given in Å.

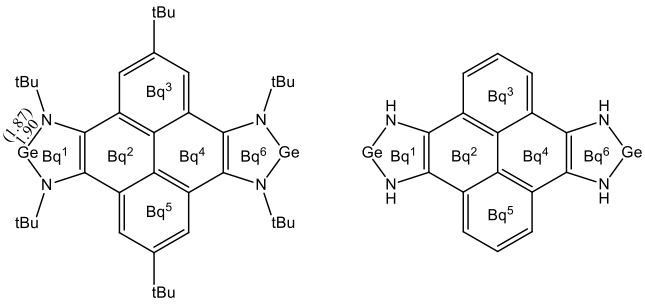

Figure S24. NICS(0) values for **2**, **2[a]** (low energy isomer of **2**), and **2-H** (where *tert*-butyl groups were replaced with hydrogens).

	3	**3-H**
Bq^1	–0.56	–2.57
Bq^2	–3.87	–5.20
Bq^3	–10.26	–10.45
Bq^4	–3.87	–5.10
Bq^5	–10.26	–10.27
Bq^6	–0.56	–2.44
Bq^7	–11.83	–12.51
Bq^8	–11.83	–12.49

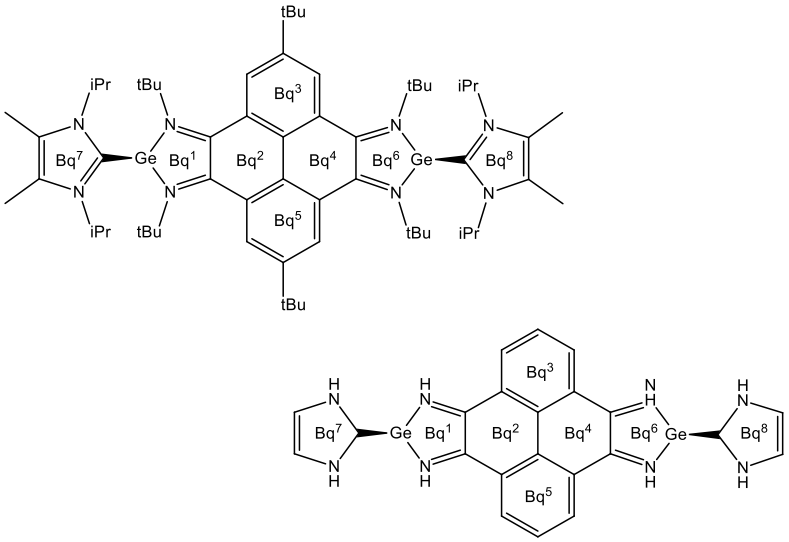

Figure S25. NICS(0) values for **3** and **3-H** (where *iso*-propyl and *tert*-butyl groups were replaced with hydrogens).

Benzene (B)

Bq^1	–8.06

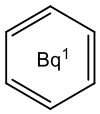

Anthracene (A)

Bq^1	–7.49
Bq^2	–11.30
Bq^3	–7.52

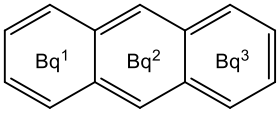

Naphthalene (N)

Bq^1	–8.54
Bq^2	–8.54

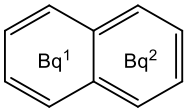

Phenanthrene (Phen)

Bq^1	–8.57
Bq^2	–5.69
Bq^3	–8.61

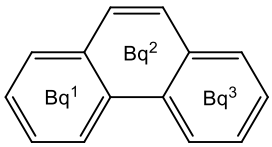

Pyrene (Pn)

Bq^1	–11.40
Bq^2	–3.99
Bq^3	–11.38
Bq^4	–4.03

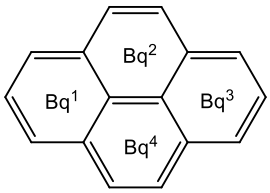

JUTPIX (JX)[28]

Bq^1	–2.63

(Expt) and computed distances of Ge-N bond given in Å.

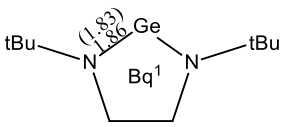

JUTPOD (JD)[28]

Bq^1	–8.74

(Expt) and computed distances of Ge-N bond given in Å.

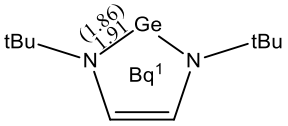

Pyrene-fused NHC (Pn_{NHC})

Bq^1	–9.40
Bq^2	–5.34
Bq^3	–10.65
Bq^4	–5.34
Bq^5	–10.65
Bq^6	–9.40

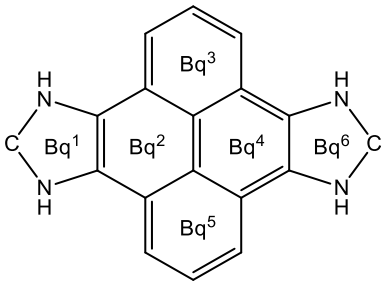

Figure S26. NICS(0) values for comparable aromatics and germylenes.

Table S5. Comparison of NICS(0) values of the reported germylenes and aromatic compounds.

	1	**2**	**2[a]**	**2-H**	**3**	**3-H**	**B**	**A**	**N**	**Phen**	**Pn**	**JX**	**JD**	**Pn_{NHC}**
Bq[1]	n.a.	–5.90	–5.85	–7.91	–0.56	–2.57	–8.06	–7.49	–8.54	–8.57	–11.40	–2.63	–8.74	–9.40
Bq[2]	–3.89	–3.66	–3.02	–4.91	–3.87	–5.20	n.a.	–11.30	–8.54	–5.69	–3.99	n.a.	n.a.	–5.34
Bq[3]	–10.66	–9.98	–10.11	–11.52	–10.26	–10.45	n.a.	–7.52	n.a.	–8.61	–11.38	n.a.	n.a.	–10.65
Bq[4]	–3.95	–2.86	–3.74	–4.92	–3.87	–5.10	n.a.	n.a.	n.a.	n.a.	–4.03	n.a.	n.a.	–5.34
Bq[5]	–10.45	–9.99	–10.11	–11.52	–10.26	–10.27	n.a.	n.a.	n.a.	n.a.	n.a.	n.a.	n.a.	–10.65
Bq[6]	n.a.	–5.83	–5.84	–7.91	–0.56	–2.44	n.a.	n.a.	n.a.	n.a.	n.a.	n.a.	n.a.	–9.40
Bq[7]	n.a.	n.a.	n.a.	n.a.	–11.83	–12.51	n.a.	n.a.	n.a.	n.a.	n.a.	n.a.	n.a.	n.a.
Bq[8]	n.a.	n.a.	n.a.	n.a.	–11.83	–12.49	n.a.	n.a.	n.a.	n.a.	n.a.	n.a.	n.a.	n.a.

**Note: A more coarse grid leads to numerical instabilities in the NICS(0) values for NICS(0) values that should be numerically identical by symmetry.*

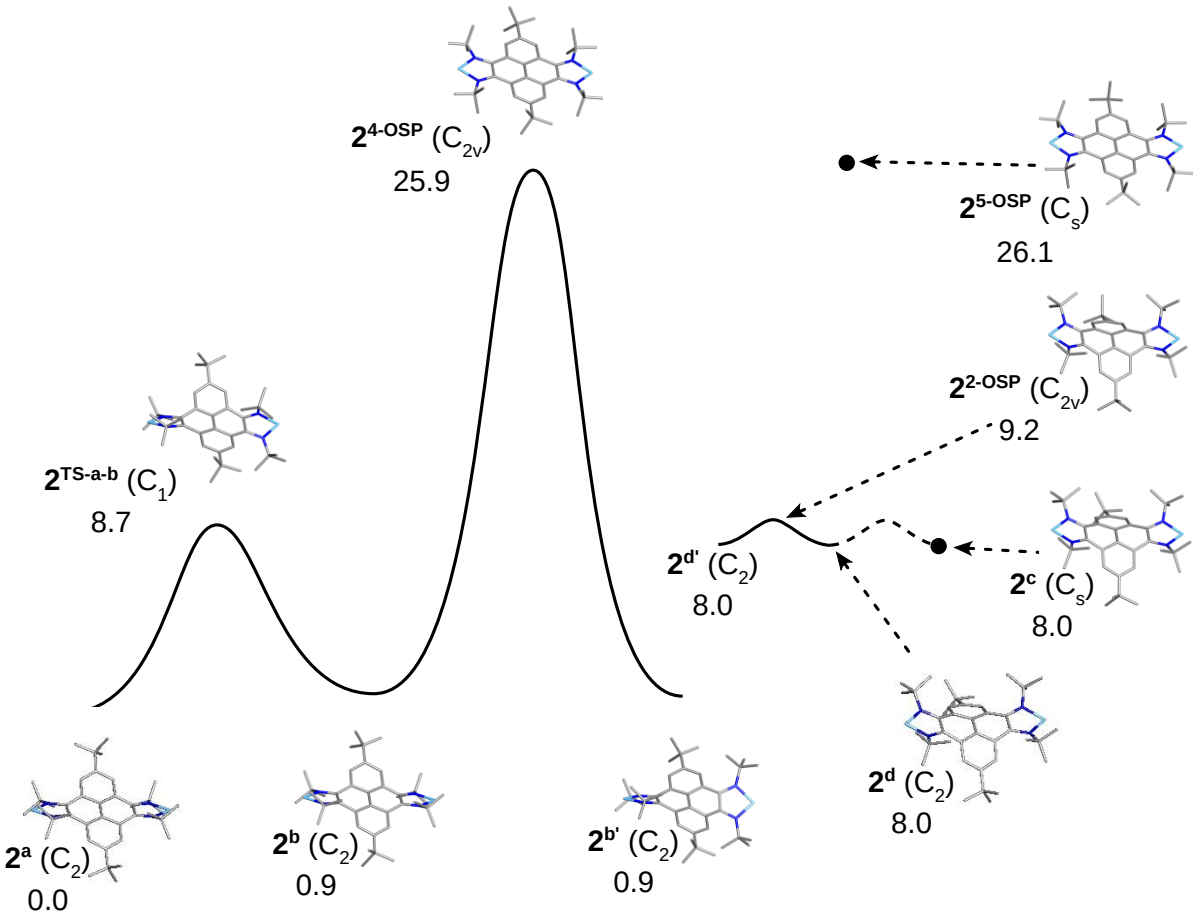

Figure S27. Potential Energy Surface (ΔE_e) for **2**. All energies reported in kcal mol^{-1}.

The potential energy surface above depicts various fluxional and higher-energy processes for compound **2**. The two lowest-energy structures for compound **2** are $\mathbf{2}^{a}$ and $\mathbf{2}^{b}$. Structures $\mathbf{2}^{a}$ and $\mathbf{2}^{b}$ are connected by a low-energy transition state $\mathbf{2}^{TS\text{-}a\text{-}b}$. While both $\mathbf{2}^{a}$ and $\mathbf{2}^{b}$ are C_2 symmetric, $\mathbf{2}^{a}$ has the same "twisting" of the germylene units where those units are staggered as observed in the geometry of the X-ray crystal structure. In $\mathbf{2}^{b}$, the germylene units are eclipsed, i.e., they are rotating in the same direction. Structures $\mathbf{2}^{b}$ and $\mathbf{2}^{b'}$ are mirror images that are connected by a high-energy C_{2v}-symmetric fourth-order saddle point ($\mathbf{2}^{4\text{-}OSP}$). Structures $\mathbf{2}^{c}$ and $\mathbf{2}^{d}$ are relatively low-energy C_s- and C_2-symmetric local minima, respectively, that buckle the pyrene core to form bowl-shaped structures, as opposed to the twisting of the pyrene in $\mathbf{2}^{a}$. The only difference between $\mathbf{2}^{c}$ and $\mathbf{2}^{d}$ is a low-energy *t*-butyl rotation. It is notable that the structure of $\mathbf{2}^{c}$ is similar to the Ge-pyrene core part of the geometry of $\mathbf{3}^{6\text{-}OSP}$. Two other higher-order saddle points ($\mathbf{2}^{2\text{-}OSP}$ and $\mathbf{2}^{5\text{-}OSP}$) exist, and the relative energy of $\mathbf{2}^{2\text{-}OSP}$ is only 9.2 kcal mol^{-1} above the lowest energy structure $\mathbf{2}^{a}$. Structure $\mathbf{2}^{2\text{-}OSP}$ connects mirror image enantiomers of $\mathbf{2}^{d}$ and $\mathbf{2}^{d'}$. Structure $\mathbf{2}^{5\text{-}OSP}$ is 26.1 kcal mol^{-1} above $\mathbf{2}^{a}$.

.

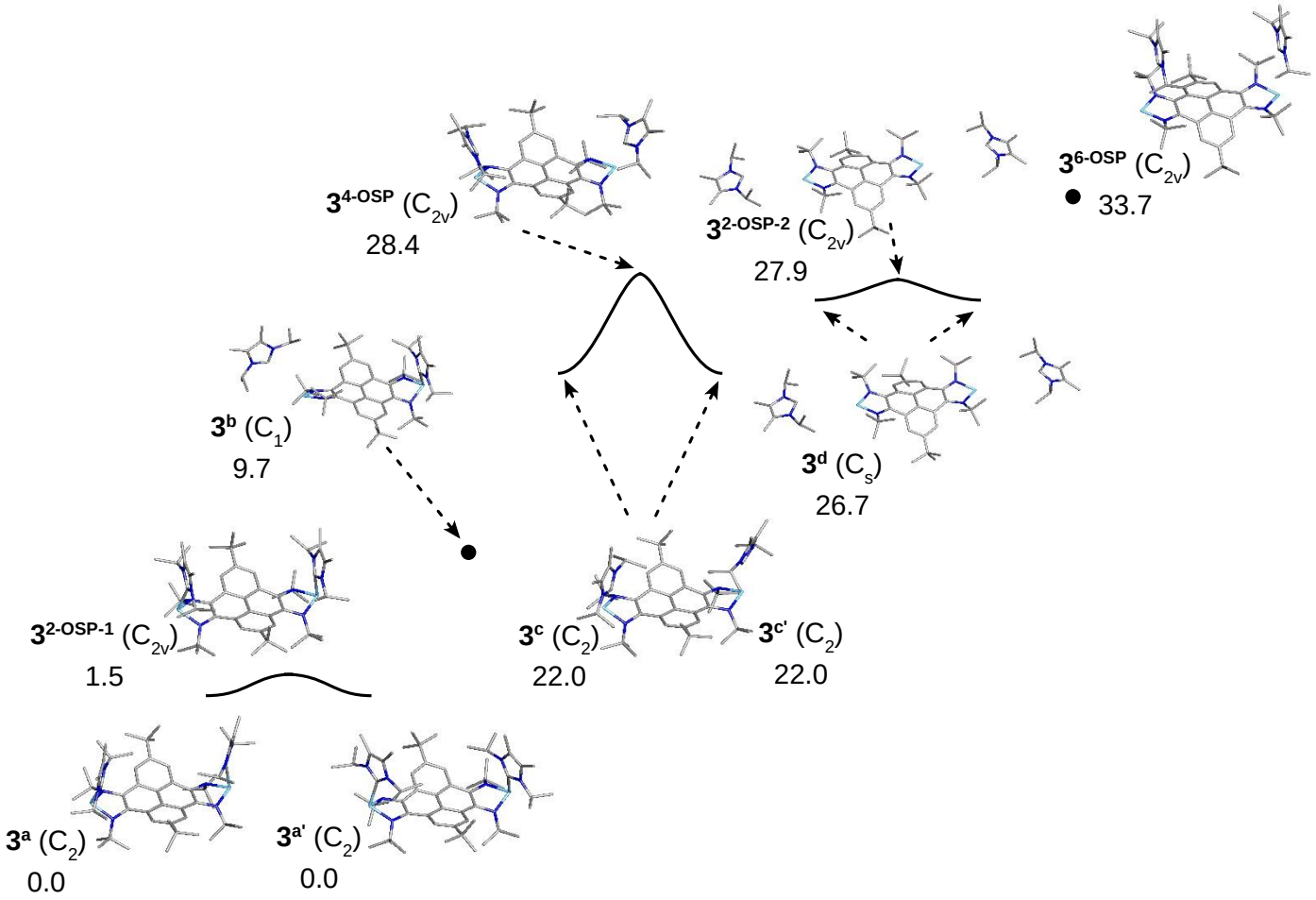

Figure S28. Potential Energy Surface for **3** (ΔE_e). All energies reported in kcal mol^{-1}.

The potential energy surface above depicts various fluxional and higher-energy processes for compound **3**. The lowest-energy structure for compound **3** is $\mathbf{3^a}$, which has C_{NHC}-Ge distances of 2.21 Å. Structure $\mathbf{3^{2\text{-}OSP\text{-}1}}$ is a low-energy C_{2v}-symmetric second-order saddle point that connects two enantiomeric C_2 structures ($\mathbf{3^a}$ and $\mathbf{3^{a'}}$). Structure $\mathbf{3^b}$ is C_1-symmetric where one of the NHCs has significantly lengthened away from the Ge-pyrene core (C_{NHC}-Ge distance of 4.12 Å), while the other NHC remains bound to the second germylene (C_{NHC}-Ge distance of 2.21 Å). Structures $\mathbf{3^c}$ and $\mathbf{3^{c'}}$ are high-energy local minimum enantiomers (C_{NHC}-Ge distances of 2.51 Å) that are connected through a fourth-order saddle point ($\mathbf{3^{4\text{-}OSP}}$ in which the Ge-C_{NHC} distances are 2.56 Å) by the double rotation of the NHCs about the Ge-C_{NHC} bond. Structure $\mathbf{3^d}$ is a C_s-symmetric structure in which both NHCs are significantly lengthened away from the Ge-pyrene core (C_{NHC}-Ge distances of 5.68 Å). A high-energy second-order saddle point ($\mathbf{3^{2\text{-}OSP\text{-}2}}$) connects two equivalent structures of $\mathbf{3^d}$ through a motion of *t*-butyl rotation. Structure $\mathbf{3^{6\text{-}OSP}}$ is a C_{2v}-symmetric high-energy sixth-order saddle point with significantly lengthened C_{NHC}-Ge distances of 5.59 Å. Interestingly, the geometry of the Ge-pyrene core in $\mathbf{3^{6\text{-}OSP}}$ has a strong resemblance to the geometry observed in $\mathbf{2^d}$ (see overlay, *vide infra*).

Table S6. ΔE_e and ΔG of **2** and **3** (kcal mol^{-1}).

	ΔE_e	ΔG
$\mathbf{2}^{a}$	0.0	0.0
$\mathbf{2}^{TS\text{-}a\text{-}b}$	8.7	9.4
$\mathbf{2}^{b}$	0.9	0.4
$\mathbf{2}^{4\text{-}OSP}$	26.0	34.6
$\mathbf{2}^{b'}$	0.9	0.4
$\mathbf{2}^{c}$	8.0	6.8
$\mathbf{2}^{d}$	8.0	7.6
$\mathbf{2}^{2\text{-}OSP}$	9.2	9.8
$\mathbf{2}^{d'}$	8.0	7.6
$\mathbf{2}^{5\text{-}OSP}$	26.1	34.9
$\mathbf{3}^{a}$	0.0	0.0
$\mathbf{3}^{2\text{-}OSP\text{-}1}$	1.5	4.6
$\mathbf{3}^{a'}$	0.0	0.0
$\mathbf{3}^{b}$	9.7	3.4
$\mathbf{3}^{c}$	22.0	21.9
$\mathbf{3}^{4\text{-}OSP}$	28.4	31.2
$\mathbf{3}^{c'}$	22.0	21.9
$\mathbf{3}^{d}$	26.7	3.4
$\mathbf{3}^{2\text{-}OSP\text{-}2}$	27.9	6.9
$\mathbf{3}^{6\text{-}OSP}$	33.7	27.4

The above data tabulates the ΔE_e and ΔG of **2** and **3** in kcal mol^{-1}. Because the Ge-pyrene core of structures $\mathbf{2}^{2\text{-}OSP}$ and $\mathbf{3}^{6\text{-}OSP}$ are quite geometrically similar, it is interesting to compare the relative energetics to their respective lowest-energy structures. Structure $\mathbf{2}^{2\text{-}OSP}$ is only 9.8 kcal mol^{-1} higher in energy than $\mathbf{2}^{a}$ while structure $\mathbf{3}^{6\text{-}OSP}$ is 27.4 kcal mol^{-1} higher than $\mathbf{3}^{a}$. This difference in energy indicates that the Ge-bound NHCs in **3** significantly increase the activation energy of the fluxional processes of **3**. It should be noted that the ΔG values of $\mathbf{3}^{d}$ and $\mathbf{3}^{2\text{-}OSP\text{-}2}$ are artificially significantly lower than their corresponding ΔE_e values because of the large separation between the units in the computation (two NHCs and the Ge-containing pyrene core), making the system more entropically favored, but still higher in energy than $\mathbf{3}^{a}$.

Structural Comparisons

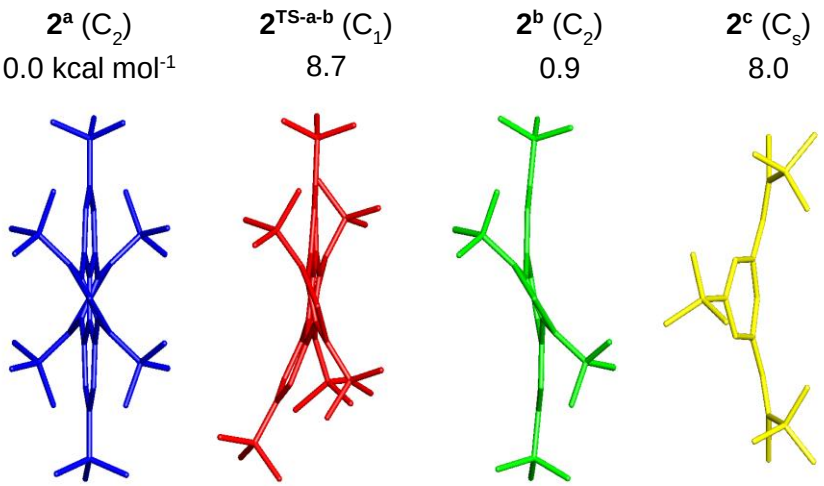

Figure S29. Structural comparison of $\mathbf{2}^{a}$ (blue), $\mathbf{2}^{TS\text{-}a\text{-}b}$ (red), $\mathbf{2}^{b}$ (green), and $\mathbf{2}^{c}$ (yellow) with a view down the axis containing the two Ge. Hydrogen atoms not shown for clarity.

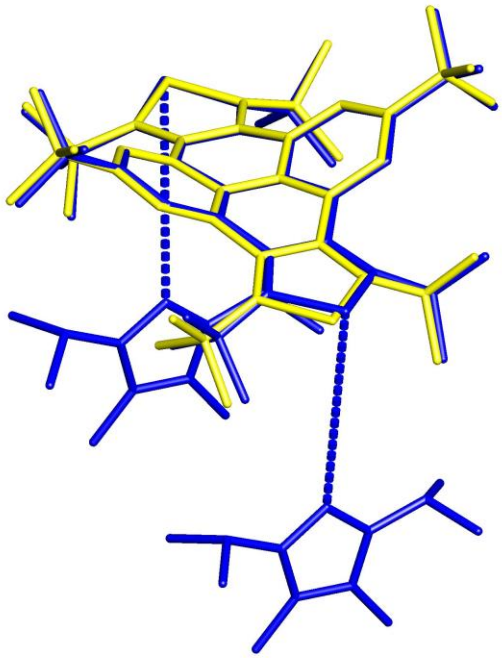

Figure S30. Structural overlay comparing $\mathbf{2}^{2\text{-}OSP}$ (yellow) and $\mathbf{3}^{6\text{-}OSP}$ (blue). In $\mathbf{3}^{6\text{-}OSP}$, the Ge-$C_{NHC}$ distance is quite long at 5.59 Å.

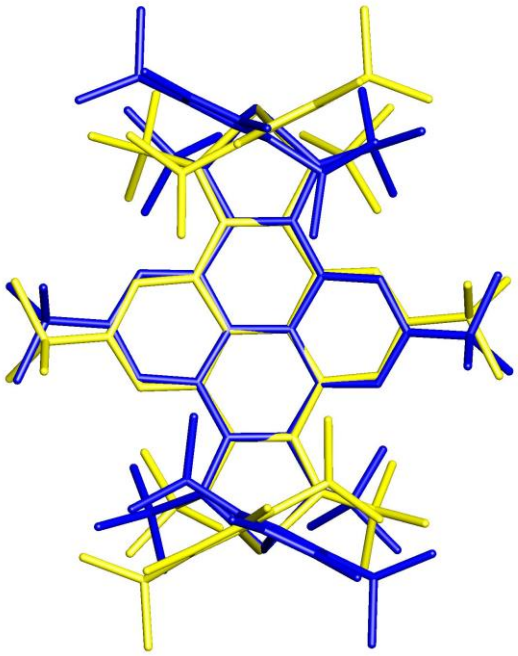

Figure S31. Structural overlay of the mirror image structures **3**^{a} (blue) and **3**$^{a'}$ (yellow).

References

1. A. J. Arduengo, R. Krafczyk, R. Schmutzler, H. A. Craig, J. R. Goerlich, W. J. Marshall and M. Unverzagt, *Tetrahedron*, 1999, **55**, 14523-14534.

2. Z. H. Wu, Z. T. Huang, R. X. Guo, C. L. Sun, L. C. Chen, B. Sun, Z. F. Shi, X. Shao, H. Li and H. L. Zhang, *Angew. Chem. Int. Ed.*, 2017, **56**, 13031-13035.

3. N. Kuhn and T. Kratz, *Synthesis*, 1993, **1993**, 561-562.

4. Bruker (2012). *Saint; SADABS; APEX3*. Bruker AXS Inc., Madison, Wisconsin, USA.

5. Sheldrick, G. M. (2015). *Acta Cryst.* A**71**, 3-8.

6. Dolomanov, O. V.; Bourhis, L. J.; Gildea, R. J.; Howard, J. A. K.; Puschmann, H. *J. Appl. Cryst.* (2009). **42**, 339-341.

7. Spek, A. L. *Acta Crystallogr. Sect C: Struct. Chem.* **2015**, *C71*, 9-18.

8. M. J. Frisch, G. W. Trucks, H. B. Schlegel, G. E. Scuseria, M. A. Robb, J. R. Cheeseman, G. Scalmani, V. Barone, G. A. Petersson, H. Nakatsuji, X. Li, M. Caricato, A. V. Marenich, J. Bloino, B. G. Janesko, R. Gomperts, B. Mennucci, H. P. Hratchian, J. V., and D. J. F. Gaussian 16, Revision B.01. Gaussian, Inc: Wallingford, CT 2016.

9. Hariharan, P. C., and Pople, J. A. *Theor. Chim. Acta* **1973**, *28*, 213–222.

10. Hehre, W. J., Ditchfield, R., and Pople, J. A. *J. Chem. Phys.* **1972**, *56* (5), 2257–2261.

11. Petersson, G. A., and Al-Laham, M. A. *J. Chem. Phys.* **1991**, *94*, 6081–6090.

12. Check, C. E.; Faust, T. O.; Bailey, J. M.; Wright, B. J.; Gilbert, T. M.; Sunderlin, L. S. *J. Phys. Chem. A* **2001**, *105*.

13. Wadt, W. R.; Hay, P. J. *J. Chem. Phys.* **1985**, *82*.

14. Clark, T.; Chandrasekhar, J.; Spitznagel, G. W.; Schleyer, P. V. R. *J. Comput. Chem.* **1983**, *4* (3), 294–301.

15. Krishnan, R.; Binkley, J. S.; Seeger, R.; Pople, J. *J. Chem. Phys.* **1980**, *72* (1), 650–654.

16. Curtiss, L. A.; McGrath, M. P.; Blaudeau, J.-P.; Davis, N. E.; Binning, R. C.; Radom, L. *J. Chem. Phys.* **1995**, *103*.

17. Schleyer, P. von R.; Maerker, C.; Dransfeld, A.; Jiao, H.; van Eikema Hommes, N. J. R. *J. Am. Chem. Soc.* **1996**, *118* (26), 6317–6318.

18. James R. Cheeseman, Gary W. Trucks, T. A. K.; Frisch, M. J. *J. Chem. Phys.* **1996**, *104*, 5497.

19. McWeeny, R. *Phys. Rev.* **1962**, *126* (3), 1028–1034.

20. Ditchfield, R. *Mol. Phys.* **1974**, *27* (4), 789–807.

21. Wolinski, K.; Hinton, J. F.; Pulay, P. *J. Am. Chem. Soc.* **1990**, *112* (23), 8251–8260.

22. A. D. Becke. *J. Chem. Phys.* **1993**, *98*, 5648.

23. Lee, C.; Yang, W.; Parr, R. G. *Phys. Rev. B* **1988**, *37* (2), 785–789.

24. Marques, M. A. L.; Gross, E. K. U. *Annu. Rev. Phys. Chem.* **2004**, *55* (1), 427–455.

25. Hall, M. B.; Fenske, R. F. *Inorg. Chem.* **1972**, *11* (4), 768–775.

26. Bursten, B. E.; Jensen, J. R.; Fenske, R. F. *J. Chem. Phys.* **1978**, *68*, 3320.

27. Manson, J.; Webster, C. E.; Perez, L. M.; Hall, M. B. JIMP 2. https://www.chem.tamu.edu/jimp2/

28. Herrmann, W. A.; Denk, M.; Behm, J.; Scherer, W.; Klingan, F.-R.; Bock, H.; Solouki, B.; Wagner, M. *Angew. Chemie Int. Ed. English* **1992**, *31* (11), 1485–1488.